GFAP Degradation in TBI:
Linking Novel Modified Products to Astrocyte Pathology and Patient Outcome

Ina-Beate Wanner[1*], Julia Halford[1], Jonathan Lopez[1], Sean Shen[2], Yu Chen[3], Hayden Zhao[1], Carolina Salas[1], Rachel R. Ogorzalek Loo[2], Steven Robicsek[4], Benjamin M. Ellingson[5], Jeffrey Gornbein[6], Timothy E. Van Meter[7], Gerry Shaw[8,9], Joseph A. Loo[2], and Paul M. Vespa[10].

Author affiliations:
2: Dept. of Chemistry and Biochemistry, Molecular Biology Institute, David Geffen School of Medicine, UCLA, Los Angeles, CA, USA.
3: Molecular Instrumentation Center (MIC), Dept. of Chemistry and Biochemistry, UCLA, Los Angeles, CA, USA.
4: Dept. of Anesthesiology, University of Florida, Gainesville, FL 32610-0254, USA.
5: Dept. of Radiological Sciences, Geffen School of Medicine, UCLA, Los Angeles, CA, USA.
6: Dept. of Computational Medicine, Statistics Core of the Dept of Medicine, School of Public Health, UCLA, Los Angeles, CA, USA.
7: BRAINBox Solutions, Inc., Richmond, VA 23219, USA.
8: Dept. of Neuroscience, University of Florida College of Medicine, Gainesville, FL 32610, USA.
9: EnCor Biotechnology Inc., Gainesville, FL, 32608, USA.
10: Dept. Neurology and Neurosurgery, BIRC; David Geffen School of Medicine, Ronald Reagan Medical Center, UCLA, Los Angeles, CA, USA.

Correspondence to: Ina-Beate Wanner
1: Semel Institute for Neuroscience and Human Behavior, Intellectual and Developmental Disability Center (IDDRC); Brain Injury Research Center (BIRC); 635 Charles E. Young Drive South, NRB315, David Geffen School of Medicine, UCLA, Los Angeles, CA 90095, USA;
Primary email: IWanner@mednet.ucla.edu Alternative email: iwanner@g.ucla.edu

Running title: GFAP degradome and astrocyte pathology in TBI

Keywords: neurodegeneration, neurotrauma, pathomechanism, biomarker trajectory, proteolysis, astroglial intermediate filament, proteostasis, proteinopathy, fragment, PTM profiling, TBI signature, epitope mapping, astrocyte, dystrophy, calpain, caspase, context of use; monitoring.

Abstract

Background: Traumatic brain injury (TBI) is a major public health concern that demands effective patient monitoring to mitigate secondary complications and improve recovery. TBI increases the risk for neurodegeneration by destabilizing proteostasis that increases protein degradation and proteinopathy. Despite the clinical importance of noninvasive TBI biomarkers, such as glial fibrillary acidic protein (GFAP), their mechanistic and cytological underpinnings remain poorly understood, hence are addressed here.

Methods: Deep proteomic profiling of GFAP used mass spectrometry (MS) sequencing of immunopurified GFAP breakdown products (BDPs) in TBI patients' cerebrospinal fluid (CSF) and serum. A unique trauma culture model used human neocortical astrocytes for GFAP epitope mapping and GFAP-BDP compartmental localization. Immunofluorescence, protease inhibitors (calpeptin, ZVAD-FMK), and live protease reporters document GFAP proteolysis and citrullination in dye-uptake-identified membrane-wounded astrocytes. Temporal profiles of GFAP and GFAP-BDPs were measured in TBI patients' CSF via calibrated, sub-saturated immunoblot densitometry. Fragment-specific prediction of six-month recovery used the Extended Glasgow Outcome Scale (GOSE).

Results: GFAP-BDP sequence sets with mapped posttranslational modifications (PTMs, citrullinations and acetylations) were identified in TBI patients' biofluids. Citrullinated GFAP profiles were distinct from unmodified GFAP in TBI patients' CSF. Novel TBI-specific cleavage fragments differed from those of Alzheimer's and Alexander diseases.

Antibody mapping in the culture trauma model confirmed GFAP-BDPs, identified a new trauma cleavage region and revealed GFAP rod-domain harbored coil1-BDPs were selectively released into fluids, while coil2-BDPs remained as intracellular aggregates. Citrullinated coil2-BDPs formed non-filamentous aggregates in dystrophic astrocytes. Calpains and caspases contributed to trauma-generated GFAP-BDPs that were active in distinct astrocyte morphotypes and injury states.

TBI patient GFAP proteolysis trajectories show that full-length GFAP and 45-49kDa fragments peaked acutely, then declined, whereas calpain-generated 37-39kDa BDPs remained elevated. Small GFAP-BDP-levels were imbalanced from expected proportions, with 20-26kDa products exceeding 15-19kDa products in CSF, consistent with preferential coil1-BDP release and coil2 retention shown in vitro. GFAP fragment profiles, but not those of uncleaved GFAP, predicted good versus poor outcome of TBI patients.

Conclusion: These findings highlight the translational importance of novel proteomic GFAP proteolysis profiles that could serve in neurocritical care monitoring. GFAP use as fluid biomarker, tied to astroglial proteinopathy, is relevant to post-traumatic neurodegeneration.

Background

Traumatic brain injury (TBI) affects 56 million people worldwide annually; nearly one in five U.S. adults have a lifetime history of TBI, making it the most common neurological disorder [1, 2]. More than half of mild TBI and 85% of moderate-to-severe patients fail to achieve long-term recovery [3, 4]. TBI nearly doubles the lifetime risk (22-29%) for neurodegenerative disease, a public health challenge that grows as populations age [5]. While the link between TBI and dementia is established, molecular mechanisms underlying this progression are less clear [6]. Early detection of brain-altering protein changes after TBI is essential and depends on sensitive biomarkers. Defining pathological early-stage TBI pathological proteoforms associated with biomarkers will facilitate risk assessment through monitoring to capture emerging signatures that may develop into post-TBI neurodegeneration [5, 7].

A pathological hallmark of neurodegenerative disease is accumulation of toxic proteoforms resulting from maladapted protein homeostasis, including amplified protein posttranslational modifications (PTMs) and degradation [8-10]. Deranged proteostasis is also a prominent consequence of TBI, triggered by rapid and sustained calcium elevation due primarily to excitotoxicity and membrane disruption. Increased proteolysis with rapid, specific postinjury profiles of calpain and caspase activation are well-documented in pre-clinical TBI models [11-15]. While tau, ß-amyloid and α-synuclein proteinopathies are known in neurodegeneration and TBI, deranged proteostasis plausibly affects many more proteins. Early noninvasive monitoring requires

understanding the relationship between cell and biofluid proteoforms to link evolving neurodegenerative processes with a diagnostic signature. While imaging and postmortem studies can confirm advanced proteinopathies, tools to monitor their early initiation after TBI remain underdeveloped. As proteolysis and altered PTMs emerge from early TBI pathophysiology, their study and detection are critical for evaluating pathogenic conversion and recovery [16, 17].

Two strategies that may capture a pathological conversion of TBI toward neurodegeneration are: 1) linking early-elevated TBI biomarkers to neuropathology [18], or 2) investigating pathological changes in TBI biomarkers themselves. Post-injury proteolysis has been reported, occurring through calpain and caspase-specific αII-spectrin breakdown products (SBDPs), but their translation into clinically useful biomarkers is limited by their ubiquitous expression [19-22]. In contrast, astroglial intermediate filament glial fibrillary acidic protein (GFAP) is highly brain-enriched and extensively studied as a TBI biomarker: GFAP fluid levels are elevated with intracranial injuries [23-25]. Circulating fluid GFAP levels rise fast, peak 6-18h postinjury, and then decline [26-29]. Elevated serum GFAP predicts poor outcome and mortality [29-32]. GFAP blood testing is FDA approved within a narrow context of use (COU) [24, 33], and is incorporated into the new National Institute of Neurological Disorders and Stroke (NINDS) TBI classification framework, reflecting its growing role in clinical TBI evaluation [34, 35]. While well-established as an acute diagnostic biomarker, longitudinal monitoring of altered GFAP proteoforms that may track deranged proteostasis remains an open priority [36-38].

GFAP breakdown products (BDPs) are in biofluids after TBI and are reportedly detected in commercial GFAP assays, yet TBI-specific GFAP-BDP sequences, and their degradation kinetics are undefined [27, 39, 40]. Can pathological GFAP-BDP proteolysis be tracked after TBI? What connects GFAP biomarker signals to proteinopathy? The mechanistic link between biofluid GFAP signals and its astrocytic proteoforms after TBI remains undefined, beginning with the paradox of this cytoskeleton-tethered protein's acute release [41]. In neuropathology, GFAP upregulation is widely used as a reactive astrogliosis indicator, yet trauma-release occurs faster than de novo expression [42-44]. GFAP modification, misfolding, and degradation have detrimental consequences for astrocytes [43, 45, 46]. Those consequences are critical because astrocytes are indispensable for intact neurovascular coupling, integrity of the blood-brain barrier, metabolite support, neural network function and memory formation. Astrocyte degeneration and their injury states after trauma are just beginning to be acknowledged [27, 47, 48]. The relevance of GFAP proteinopathy is underscored by Alexander disease, a progressive neurodegenerative disease that is causally linked to toxic GFAP aggregates and fragments in degenerating astrocytes [49-51], also leading to elevated GFAP in biofluids [51-56]. Clarifying GFAP degradation and modification in both TBI biofluids and injured astrocytes is critical to improving biomarker interpretation and outcome prediction.

To start bridging these translational gaps, we performed deep proteomic sequencing of immunopurified GFAP fragments in TBI patient cerebrospinal fluid (CSF). These studies established GFAP proteolysis profiles in TBI patients, which were confirmed by a human trauma culture model for mechanistic and imaging studies. Our work defines novel TBI patient-specific GFAP fragments and PTMs, with a unique trauma-cleavage that was further validated by antibody epitope mapping in the trauma model. Importantly, distinct GFAP-BDPs are shown selectively released or retained in injured astrocytes, directly linking fluid biomarker signals to astrocyte proteinopathy through shared origin. These findings advance the molecular understanding of GFAP dynamics post-TBI and may open new methods for detecting neurodegeneration-associated astrocyte pathology in neurotrauma.

Methods

TBI patients' demographic and clinical data and brain tissue specimen procurement

This observational DANA foundation funded cohort study included 112 CSF samples and 3 serum samples from 26 consented adult TBI patients admitted to neurocritical care at level one trauma centers at UCLA and at the University of Florida, Gainesville, and a commercial control serum sample (Precision Med; Additional File1 Tables S1, S2). Patient median age was 40±19 years, 22 subjects were male and 4 were female, and median score on the Glasgow Coma Scale (GCS) was 6 ±3.4. Enrollment occurred between 2018-2023 and included anonymous demographic and clinical parameters (Additional File1 Table S1). The human subjects protocols included local IRBs that approved informed consent procedures from two medical centers (1) the UCLA Ronald Reagan Hospital Neuro-Intensive Care Unit under Chair Paul Vespa and (2) the University of Florida Dept of Anesthesiology under Steven Robicsek, Medical Director Intraoperative Neuromonitoring. The UCLA Office of the Human Research Protection Program (OHRPP) Institutional Review Board (IRB) approved the informed consent protocol (BIRC-IRB) for deidentified CSF and serum collection as well as clinical data sharing and also declared per HS-7 exemption amendment the use of pathology pre-shelved fetal brain specimen donation (see below). All except two patients had recovery scores on the Glasgow Outcome Scale (GOS) reported both at hospital discharge and by phone interview at six-month postinjury on extended GOS (GOSE). Deidentified human fetal brain tissue from voluntarily aborted pregnancies was donated adhering to stringent ethical regulations. They were preshelved, with approved exempt from IRB-review at the UCLA Translational Pathology Core Laboratory (Sara Dry, Chair of Pathology and Laboratory Medicine). Consent was established through UCLA Dept of OB-GYN (Angela Chen, Division Chief of Family Planning). Signed informed consent occurred after decision on elective termination, complying with US Public Law 103-43 and NIH policy, ensuring no incentive (The Public Health Service Act, 42 U.S.C. § 289g-2). Cerebral astrocyte cultures were prepared from 17 donated human fetal cranial specimen aged 16-19.5 gestational weeks.

Immunoprecipitation and mass spectrometry sequencing of GFAP from TBI patients

Mass spectrometry (MS) experiments were performed on six cerebrospinal fluid (CSF) and serum samples from five TBI patients. GFAP was immunoprecipitated using a rabbit polyclonal anti-GFAP antibody that was cross-linked to protein G conjugated magnetic beads (Dynabeads) using dimethylpimelimidate-2 (freshly prepared 20mM DMP in 200mM triethanolamine, pH8.6) followed by heat/ice denaturing and reduction in 1% ß-mercaptoethanol [57-59]. Eluted material was separated by preparative SDS polyacrylamide gel electrophoresis (SDS-PAGE) using 10% NuPAGE gradient gels in morpholinoethansulfonic acid buffer in reducing conditions along with a molecular weight standard (Benchmark). Gels were Sypro-Ruby stained and fixed in 10% methanol, 7% acetic acid. GFAP bands were cut out under UV light and placed into tubes for in-gel trypsin digestion. A fraction (~1/9th) of the eluate was blotted and GFAP was detected using a mouse monoclonal antibodies (mabs) to GFAP (mab1A64-244, Abbott Diagnostics or MCA3E10, EnCor Biotechnology Inc., Additional File1 Table S3) to provide reference signals for gel band excision. Bands at 50 and 25kDa were omitted to avoid immunoglobulins (Additional File1 Figure S1). Gel bands were fully destained, dried, and then reduced with 10mM tris(2-carboxyethyl) phosphine in 100mM ammonium bicarbonate buffer at 56°C for 30min followed by alkylation with 100 mM iodoacetamide in the same buffer at 37°C for 15min. The bands were equilibrated with acetonitrile (ACN), dried, and digested using 0.01mg/ml

sequencing grade trypsin in 100mM ammonium bicarbonate buffer at 37°C for 12h. Peptides were extracted from the gel bands by three rinses of 50% ACN/0.1% formic acid solution at 37°C for 15min and the combined extracts were dried in a vacuum concentrator. The peptides were measured by liquid chromatography-tandem MS (LC-MS/MS) using an Ultimate 3000 nano-LC instrument (1h gradient) coupled to a Q-Exactive Plus Orbitrap mass spectrometer. Full spectra (MS1) were collected at a resolution of 70,000 and the 15 most abundant ions of each scan were subsequently fragmented by higher-energy collisional dissociation (HCD; MS2) with a resolution of 17,500 and a dynamic exclusion of 45s. Digestion of defined amounts of recombinant human GFAP served as technical controls (Additional File1 Figure S2). MS data were searched against the human GFAP protein sequence (Uniprot (https://www.uniprot.org/uniprotkb/P14136/entry) via Proteome Discoverer (PD) version 1.4. SEQUEST-engine confirmed peptides were unique to GFAP (not shared by e.g. vimentin, neurofilaments). "High" confidence peptides (green on maps) had at least two peptides filtered using ≤1% false discovery rate (FDR) threshold of cross-correlation (X-corr) scores for peptide matches contingent on ion precursor charge states. Few "medium" confident peptides (yellow) had at least two peptides with ≤5% FDR (Figure 1; Additional File1 Table S4). Identified PTMs included acetylation and citrullination that were further validated by: (a) a unique signatures of citrullination (immonium ion at m/z 130.0975 and/or neutral loss of isocyanic acid at 43.0058Da) or lysine acetylation (cyclized immonium ion at m/z 126); (b) a MS2 product of b- and y-ions documented mass increments consistent with modifications (Additional File1 Figure 9); (c) a comparison of identified citrullination sites after treatment with peptidylarginine deiminase (PAD) enzyme [60].

Partial chemical cleavage of GFAP for monoclonal antibody epitope mapping

The binding region of mab anti-GFAP clone 5C10 was determined initially by binding to the peptide covering amino acids (aa) 233-261 of the human coil2A sequence (AALKEIRTQYEAMASSNMHEAEEWYRSKF) using dot blots. The specific epitope was subsequently identified using partial chemical cleavage at tryptophan, which there is only one in GFAP, aa W256. Recombinant GFAP (33µg) was treated in excess with 1% BNPS-Skatole (100µg; 1mg/ml glacial acetic acid; 3-bromo-3-methyl-2-(o-nitrophenylsulfenyl)indolenine, Sigma), an oxidant and brominating agent selectively cleaving proteins at tryptophan residues [61, 62]. An equal volume of distilled water precipitated BNPS-Skatole that was removed by centrifugation (5min at 12,000rpm). The supernatant was lyophilized and the GFAP and tryptophan-cleaved BDPs were separated by SDS-PAGE, blotted followed by mab incubation of MCA-5C10 or MCA-3E10, a coil1 GFAP antibody, and a pan-intermediate filament antibody, IFA (hybridoma supernatant from ATCC, epitope coil2B aa 358-377: ALDIEIATYRKLLEGEENRI; see Additional File1 Figure S5) [63, 64].

Western blotting using scaled densitometry and GFAP calibration

SDS-PAGE was conducted as previously described using 7.5% acrylamide for αII-spectrin, 12% gels for GFAP [27]. Protease inhibitors (cocktail CompleteMini, Roche 1:50) and EDTA (10mM) were added to TBI patient CSF, samples were equilibrated to Laemmli sample buffer, boiled for 5min followed by ice incubation and ß-mercaptoethanol to 1% was added prior to loading 34 µl/lane. The same procedure was followed for astrocyte lysates and concentrated culture media described below. Samples and molecular weight standards (Kaleidoscope, Biorad) were collected upon initial run for 30min at 100V and separated for 1h at 120V until the bromophenol blue front reached the bottom. Proteins were cold transferred at 120V for 3h onto nitrocellulose and stained with Ponceau S. Membranes were blocked in 10% non-fat milk in Tris-buffered saline with Tween (TBST) at room temperature (RT) prior to incubation with primary antibody in 5% BSA in TBST overnight at 4°C. Secondary antibodies conjugated with peroxidase (Pierce) were incubated in 5% BSA in TBST for 1h at RT. Enhanced Chemiluminescence (ECL) substrate was applied to washed membranes for

5min at RT (Pico and Femto ECL, Pierce) and multiple exposures were used either of Kodak films or with an iBright imager (ThermoFisher Scientific). Calibrants were recombinant human full-length GFAP and a 20kDa His-tagged GFAP-BDP (aa 72-217, EnCor Biotechnology Inc.) diluted with 0.5% BSA in TBS at defined concentrations (0.08-2.6ng) that were measured at different exposures (Additional File1 Figure S11, Table S5). Densitometry was performed on eight exposures from each blot (2s-20min) after background correction. Subsaturated band measurements were standardized to 1min by multiplying shorter exposures and by dividing longer exposures using scaling factors between exposures that were empirically determined from same unsaturated between two exposures (Additional File1 Table S5). Band sizes were computed using distances of each molecular weight marker from the gel-front and curve-fit equations.

Human cortical astrocyte cultures, trauma, sample preparation and microscopic imaging

The human culture trauma model: In vitro differentiated fetal neocortical astrocytes were prepared as previously described [65]. Briefly, cortical tissue was mechanically dissociated, filtered and astrocytes were enriched by Percoll gradient centrifugation. Cells were expanded in DMEM/F12 with 10% fetal bovine serum (FBS). Residual oligodendrocytes and progenitor cells were removed by shaking. Astrocytes were seeded on collagen-I coated deformable silastic membranes at 138,000-180,000 cells/9.62cm^2 and differentiated in DMEM/F12: Brainphysiology Medium Additional File1emented with SM1 and N2A (Stem Cell Technologies) by stepwise serum removal. Astrocytes were traumatized by 50ms pressure pulses (4.9-5.3psi) that abruptly stretched the culture bottom, shearing the cells compromising membrane integrity that led to delayed cell death [27].

Live microscopy imaging: Cerebral fetal human brain cells were differentiated for three weeks by serum withdrawal in a 1:1 mixture of DMEM/F12: Brainphysiology medium (StemCell Technology). Live imaging was done 5h after stretch injury on a Leica DMI8 microscope in a gas and temperature-controlled chamber (Okolab). Cells were bathed for 5min in 60µM propidium iodide (PI, Sigma) to label leaky membranes. Washed cultures were live-imaged in the presence of two permeable fluorescent protease substrate reporters for calpains (30µM CMAC tBoc Leucyl-methionine, ThermoFisher), and for caspases (5µM DEVD-NucView488, Biotium).

Astrocyte protein sample preparation for gel electrophoresis: Whole cell lysate (WCL) of adherent astrocytes was prepared by adding 150µl lysis buffer/9.62 cm^2 wells (150mM NaCl, 20mM Tris, 5mM EDTA, 10mM NaPyrophosphate, 30mM phosphatase substrate, 5mM dithiothreitol, DTT (Calbiochem)), 1% NP40 and 1 tablet/10ml protease inhibitors (Mini Protease Inhibitor Cocktail, Roche). Lysis buffer was incubated for 5min at 4°C, lysates were collected by scraping into low binding tubes and homogenized by 3x5s sonification bursts without foaming (Branson Digital Sonifier, 90% or constant amplitude duty cycle, output level 5). Culture medium (CM) without serum or protein Additional File1ements was collected and 5mM DTT and 1tablet protease inhibitors /10ml added. Particles from lifted cells and debris were pelleted by initial centrifugation (5000g, 5min, 4°C) and then lysed for 5-10min in 0.5% lysis buffer followed by 3x5s sonication. Remaining insoluble fractions were removed by centrifugation (10min at 16,000g 4°C). Media were concentrated (Vivaspin, 3kDa cutoff) by centrifugation (4-8h at 5000g, 4°C) to ~1/10th-20th of the original volume to obtain a protein concentration of 1-1.5 µg/ml. All samples were immediately frozen in aliquots at -80°C.

Antibodies used on TBI CSF and astrocyte samples

All antibodies are tabulated with known epitopes, sources, dilutions and RRIDs (Additional File1 Table S3). A rabbit polyclonal GFAP antibody (DAKO) was used for immunoprecipitation and immunoblotting. For densitometry the antibody was applied initially at a high dilution (1:20,000-150,000) for detecting full-size GFAP and large GFAP-BDPs, followed by a lower dilution (1:5,000-7,000) for detecting small GFAP-BDPs, which were adjusted in subsequent scaling. MCA-3E10 was generated to a recombinant construct containing aa 72-217 of human GFAP, comprising coil1A and 1B. The epitope for MCA-3E10 was localized to aa 196-210 (EIRFLRKIHEEEVRE), using peptide competition with a set of 20 nested aa peptides, each overlapping by 5 aa. Additional mabs were MCA-5C10 (EnCor Biotechnology Inc.), 1A64-244 (Abbott Diagnostics), a mixture of three clones (4A11, 1B4, 2E1, BD Pharmingen) and mab GA5 (Sigma [54, 66]). Citrullination studies used clone CTGF-1221 that was kindly provided by Akihito Ishigami (Professor, Tokyo Metropolitan Institute for Geriatrics and Gerontology) to detect citrullinated GFAP (cit-GFAP) at aa sites R270 and R416 [67]. Anti-peptidyl-citrulline antibody clone F95 (EMD Millipore) validated citrullinations. Several additional rabbit polyclonal citrullination site-specific GFAP antibodies, including cit-GFAP-270, were generated and characterized (BRAINBox Solutions, Inc.). A mab against αII-spectrin was used at 1:3,000-1:5,000 dilution (Enzo Life Sciences).

Protease inhibition in the human trauma culture model

Pan-calpain inhibitor calpeptin (13µM Z-Leu-nLeu-H, Millipore/Sigma), a non-toxic cell-permeable peptide aldehyde inhibitor [68, 69]. Pan caspase inhibitor ZVAD-FMK (11µM benzyloxycarbonyl-Val-Ala-Asp(OMe)-fluoromethylketone (Enzo/ThermoFisher)) is a cell-permeable, irreversible pan-caspase inhibitor that is effective against a spectrum of caspases (1-10, except 2; Invitrogen) [70]. ZVAD-FMK is reported showing also calpain inhibition after controlled cortical impact to the mouse brain [71]. Inhibitors were applied 10min to cultures after stretching omitting gentamicin in the medium and were incubated with cells for 5, 24 or 48h replenishing drugs every 8-10h. Other tested calpain inhibitors included leupeptin (20µM) and SJA6017 (10µM Calpain Inhibitor VI, Calbiochem) had limited effect, were toxic by either increasing cell permeability as did PD1500606 (100µM, Calbiochem), or by increasing cell death as did MDL28170 (Z-Val-Phe-al, 4µM, Calbiochem) and were not further pursued.

Statistical analysis approaches

GFAP band measurements were assessed for normality by the Shapiro Wilk criterion for Gaussian distribution fit. GFAP and GFAP-BDP measurements deviated from normal distribution, determined by significantly lowered W-values, and were log-transformed replacing zero with half of the lower limit of detection (0.7pg or a concentration of 27pg/ml; Additional File1 Figure S12B, C).

Reproducibility: Immunoblot densitometry reproducibility was determined on technical replicates using the coefficients of variation (CV=SD/mean x100, Additional File1 Table S6). **Covariates**: Effect modifiers patient age, race, sex and concurrent body temperature, and their interactions were evaluated.

Model of variance components: Used was a restricted maximum likelihood (REML) linear mixed model (LMM) with patient identifiers (IDs) as random effect to account for repeated measures per patient. Added to the model was injury elapsed days, and knotted spline estimation.

Effect testing: For the effect of age, partial omega squared (ω_p^2) was used to report the proportion of the population variance fixed effects because it adjusts for variable sample size [72]. It was computed using fixed

effect statistic (F-statistic) results of the REML-LMM output in SAS/Jmp along with degrees of freedom (df) and its denominator term (DFDen) as follows: (1)

$\omega_p{}^2 = \mathrm{F} * \mathrm{df}_{\mathrm{effect}} - (\mathrm{df}_{\mathrm{effect}}/\mathrm{F} * \mathrm{df}_{\mathrm{effect}}) + \mathrm{DFDen} + \mathrm{df}_{\mathrm{effect}}$. (1) *Age covariate effect formula*

Temporal profiles: Longitudinal means were graphed by spline fit lines from resampled daily CSF draws along with 95% confidence intervals (CI, Figs. 7C, 8). Temporal GFAP and fragment trajectories were evaluated using REML-LMM with age as covariate (Additional File1 Table S7 and Figure S13). Cohen's D effect sizes on each postinjury day (PID) were computed using adjusted means (Adj.Means) on each PID compared with overall means weighted for sample availability on each day [73, 74] with pooled (SD) from the total random variance component (Additional File1 Table S8, Additional File1 Figure S10) [75]. Formula (2):

$\mathrm{Cohen's\ D}_{\mathrm{forGRAP\ by\ PID}} = (\mathrm{Adj.Mean}_{\mathrm{PID}} - \mathrm{Adj.Mean}_{\mathrm{Overall}})/\sqrt{pooled}\ SD$ (2) *Time effect formula*

Bivariate correlations: To assess GFAP substrate-product and product-product relationships, log-transformed GFAP band signals were pairwise correlated reporting uncorrected Pearson correlation coefficients (Figure 7, Additional File1 Figure 14). Biplots used orthogonal fit for equal variance between GFAP bands and are reported with coefficient of determination (R^2) and Benjamini-Hochberg-based FDR-corrected Logworth, [-$\log_{10}$(p-values], (Figure 9). The outlier portion is documented with robust correction defined as percent of datapoints with a distance exceeding 3X the residual SD. Correlation outliers that might affect the correlations across all variables were inspected using the Mahalanobis distance to determine potential multivariate outlier with the threshold being the upper control limit, UCL and calculated using sample size and the number of variables used, by applying robust weighting to discern outliers [76-78].

Outcome prediction: The GOSE score was used to assess six-month recovery prediction by longitudinal GFAP profiles. GFAP trajectories are shown for good (GOSE 5-8), and poor (GOSE 1-4) outcomes and were graphed using cubic splines with same curvature fit (λ= 0.28) and 95% CI (Figure 8). GFAP profiles were assessed for their ability to distinguish good versus poor outcomes using a REML-LMM model with ID as a random and elapsed PIDs (modeled with knotted splines) as a fixed effect and controlling for age. Differences in GFAP adjusted means between good and poor recovery were calculated as described as follows in formula (3).

$\mathrm{Cohen's\ D}_{\mathrm{for\ outcome}} = (\mathrm{Adj.Mean}_{\mathrm{GOSE\ poor}} - \mathrm{Adj.Mean}_{\mathrm{GOSE\ good}})/\sqrt{pooled}\ SD$ (3) *Outcome effect formula*

Cohen's D in SD units here uses total residual variant component capturing within-subject variability (Additional File1 Table S7). Figure 8D shows adjusted means using above REML-LMM model with standard errors and post-hoc t-statistic and patient ID as random effect and elapsed postinjury time as fixed effect.

Label-free MS analysis: A) Peptide presence/absence frequency was compared between coil1 and coil2 peptides using a mixed model with unequal variances, patient ID as random and GFAP-BDP sets as fixed effects. B) The peak ion abundance of coil1 versus coil2 ions was compared using a mixed model analysis with ID as random and GFAP-BDPs as fixed effect while undetected peptides were excluded (Additional File1 Figure S3).

Results

Novel set of trauma-specific GFAP breakdown products in TBI patients

GFAP fragments in TBI patients differ from Alzheimers and Alexander Disease BDPs

GFAP displays a range of degradation products and cytoskeleton proteolysis is increased in TBI [11, 27]. Thus, to determine TBI-specific GFAP degradation, we sequenced fragments from gel-slices of immunopurified GFAP using MS in six CSF samples (from five TBI patients) matched to immunoblot signals (Additional File1 Figure S1, Bandsets I-IV). Molecular masses of each size-range were estimated pooling slice-specific high-confidence peptide sequences from each patient-sample covering GFAP-BDPs (Figure 1B). Bands (I.) contained a 41.7kDa fragment. Gel-slice of Bands (II.) migrated between 36-39kDa and yielded sequenced peptides covering a calculated mass of 40.6kDa. This slightly higher mass likely resulted from pooling peptides from different patient-samples, suggesting patient-specific variability in GFAP proteolysis. In addition, remaining charged residues of the acidic GFAP may have contributed to slightly faster gel migration [79-82]. Bands (III.) comprised two GFAP-BDPs, a 21.8kDa product coil1 and a 17.5kDa product within coil2, which are alpha-helical coils of the rod domain in the GFAP center. Bands (IV.) included a slightly shorter coil1-BDP of 21.3kDa as well as a slightly shorter coil2-BDP of 15.2kDa size. These sequences indicate consecutive cleavage of coil1 and of coil2-BDPs. Coil1-covering fragments display the same N-terminus but slightly differing C-termini with a four-residue larger Band III than Band IV coil1-product (Figure 1C). Interestingly, these coil1 products extended beyond a prior reported caspase 6 cleavage (at VELD225) associated with Alexander disease [54]. The two coil2-products had the same N-terminus (F261) but distinct C-termini, with 22aa, ~2.4kDa, larger coil2-band (III., K410) and shorter coil2-band (IV., R390, Figure 1C). Immunoblots using a polyclonal antibody detected small GFAP-BDPs with these observed molecular masses, although mab MCA-3E10, specific for coil1b, missed the 17kDa band (Figure 1A, Additional File1 Figures S1, S2). Notably, the TBI patient-associated 15-17.5kDa coil2-products were smaller than the 30kDa fragment that is shown in Alzheimer's disease (AD) samples, yet they were consistent with an AD-reported caspase 3 cleavage site (aa residues 258-266, RSKFA↓DLTD) [83]. Markedly, none of these two small bandsets had peptides in the linker region between coil1B and 2A and in coil2A. However, these aa were readily detected in larger TBI-sample GFAP bands (47 and 50kDa) and in control analysis of full-length recombinant GFAP (Additional File1 Figure 2). These findings indicate stepwise and TBI-specific proteolysis produces the previously observed trauma-induced GFAP-BDPs of 42, 37 and 18-25kDa bands [27]. Finally, coil1-BDPs had greater coverage than coil2-BDPs (Figure 1B), an imbalance that was further supported by significantly higher frequency of coil1 versus coil2 peptides, which were consistently underrepresented across MS runs (Additional File1 Figure S3A, Methods). Further, ion peaks were significantly higher in coil1 over coil2 peptides also documenting greater abundance and added evidence on a biofluid imbalance between these two sets of BDPs (Additional File1 Figure S2B).

GFAP breakdown products in TBI patients' serum samples

An immunoblot of a depleted TBI serum sample shows strong 37kDa and a ~20kDa bands that were very faint in a non-TBI control sample (Additional File1 Figure S4A). We immunoprecipitated GFAP from TBI patient sera and identified a coil1-product spanning aa S51 to R217 (97 residues, 18.2kDa, Additional File1 Figure S4). With 59% sequence coverage, the termini could not be confidently identified. Noteworthy, coil2-containing peptides were missing in four different TBI blood samples from two patients.

In summary, detailed MS data document GFAP degradation in TBI differs from that of other neurodegenerative diseases and thus cannot solely be predicted from recombinant GFAP digested with purified enzymes in cell-free systems or toxin treatments [54, 83, 84]. Exhaustive MS sequence analysis of GFAP in TBI patient biofluids revealed proteolytic processing expected to generate equimolar co-products; however, coil1-products were more abundant and more robustly detected than coil2 products. This disparity was further confirmed by greater abundance of 20-23kDa bands versus 15-19kDa GFAP-BDPs in immunoblot densitometry of 24 TBI patients (Figure 8, see below). Lastly, we did not recover peptides spanning the region between coil1B and coil2B that suggests a previously uncharacterized trauma-specific cleavage site(s). To address these unresolved issues, we employed a human trauma cell culture model.

Human trauma model evidence of GFAP cleavage and distinct distribution fates of coil1 and coil2 products.

Trauma-generated GFAP coproducts are destined to different locations.
Mabs with defined GFAP epitopes were used on previously established preparations of cell and fluid samples from traumatized human primary neocortical astrocytes [27, 65]. Mechanical pressure-pulse stretching led to GFAP filament disassembly, release and degradation in traumatized astrocytes [27]. Immunoblots of WCL ("cells") and concentrated CM ("fluid") of unstretched controls and stretched cultures from the same donors were probed (Figure 2). All clones detected full-length GFAP and large fragments but differed in their detection of small BDPs (Figure 2) [85]. MCA-3E10, detected a 20kDa GFAP-BDP in astrocyte CM that increased after trauma, yet failed to detect it in cells here (Figure 2C, red). Clone GA5 detected an epitope at the end of coil2 and the beginning of the "tail" sequence [66]. GA5 detected a set of 17-28kDa GFAP-BDPs in cells but not in fluids (Figure 2C, purple). A cocktail of three mabs served as positive control, proofing GFAP-BDPs in cells and fluids from same donors (Figure 2C, blue). Thus, following mechanical trauma of human astrocytes, coil1 products were preferentially released, while coil2 products were selectively retained within cells. This new human trauma model insight helps address the unequal presence of coil1/2 BDPs in biofluids of TBI patients.

A novel GFAP trauma cleavage site is defined by an epitope mapped via partial chemical GFAP cleavage.
Clone MCA-5C10 detected full size and large GFAP fragments in cells and fluids of same donor's samples, but missed any fragment smaller than 40kDa in both compartments. This suggests that 5C10 recognized an epitope that was destroyed during trauma proteolysis of GFAP (Figure 2C, dark yellow). MCA-5C10 showed weak but reproducible binding on dot blots to aa 233-261 of the human coil2A sequence. To pinpoint its epitope, we performed a chemical-mediated partial digest of GFAP using BNPS-skatole that cleaves after tryptophan residues [61, 62]. The single tryptophan in GFAP, W256, lies within the region recognized by MCA-5C10. BNPS-skatole treated GFAP produced a N-terminal 34.6kDa and a C-terminal 20.5kDa fragment and MCA-5C10 bound avidly to the C-terminal fragment on western blots (Additional File1 Figure S5). The identity of this 20.5kDa BNPS-skatole fragment was confirmed using anti-IFA, a pan-intermediate filament antibody to coil2B (aa 358-377, ALDIEIATYRKLLEGEENRI) [63, 64]. MCA-3E10 coil1 antibody bound the N-terminal 34.6kDa BNPS-skatole fragment. This concludes that the sequence following tryptophan W256 from tyrosine 257 to tyrosine 260 (aa YRSKF), is an important component of the MCA-5C10 epitope and likely also includes elements of the neighboring caspase 3 cleavage site, (aa YRSKFA↓DLTD). The by MS identified TBI-generated coil1 sequence extended no further than R239 and the beginning of coil2 products were consistently observed F261. This unique mapping data suggests a novel trauma-pattern of cleavage(s) that occur upstream of F261 combined with potential caspase 3 activity downstream of it.

Calpains and caspases cleave GFAP and vary in activity among astrocyte types and injury states.

Calpain and caspase inhibitors block trauma-induced GFAP proteolysis

The contribution of TBI-activated calpains and caspases generating these TBI fragments was investigated by using suitable inhibitors in the trauma culture model [11, 86-88]. SBDPs served as positive controls with caspase and calpain indicator fragments, yet the protein's ubiquitous expression, (e.g., muscle, endothelial, epithelial and nucleated blood cells) limits its utility as a TBI proteolysis biomarker [15, 19-22, 89]. Human traumatized astrocytes were treated with calpain inhibitor calpeptin (C), or caspase inhibitor ZVAD-FMK (V), and GFAP-BDPs were analyzed in WCL from adherend cells, fluids, and pelleted lifted cells and debris. αII-spectrin and SBDPs were abundantly expressed in differentiated human fetal astrocytes (Additional File1 Figure S6), as is reported in human gray and white matter astrocytes [90-92]. Both, calpain (145/150kDa) and caspase (120kDa) SBDPs increased two days after stretch injury in cells, debris, and fluids and decreased by their respective inhibitors (Additional File1 Figure S6). Of note, both, calpain-SBDPs were observed as double-band in WCL, yet a single 150kDa was also found in lifted cells, while a single 145kDa band was found in fluids, respectively. The 120kDa caspase-SBDP was enriched in detached material of demised cells. These findings indicate that αII-spectrin calpain fragments, alike GFAP-BDPs, originated intracellularly, and had distinct compartment preferences after trauma, opening the possibility for selective distribution of specific cytoskeletal fragments not being unique to GFAP.

A fraction of GFAP appeared fragmented in unstretched viable cells due to baseline cytoskeleton turnover (Figure 3A) [41]. Two days post-stretching, GFAP-BDPs were elevated in cells, fluid and lifted material. Calpeptin reduced the 35-38kDa GFAP-BDP and smaller BDPs, while undigested GFAP initially accumulated in adherent cells and lifted material (Figure 3A; Additional File1 Figure S7). ZVAD-FMK effectively inhibited all 19-26kDa small BDPs. Combined inhibitors (CV) had an additive effect, confirming that both calpains and caspases were involved in TBI-initiated human GFAP degradation. This data provides the first evidence of endogenous trauma-inflicted calpain and caspase digestion of GFAP going beyond rat cell toxin-treatment mouse tissue experiments [84]. These findings link traumatic GFAP proteolysis in human astrocytes with the well-known roles of calpains and caspases in TBI and cell death processes and supports the goal of using GFAP-BDPs as CNS-specific protease biomarkers for TBI patients [93, 94].

Live imaging of proteolysis and membrane wounding captures a range of acute astrocyte injury states

To document the cellular pathophysiology after injury we imaged stretched astrocytes using fluorescent calpain and caspase reporters together with PI, a membrane permeability dye. In vitro differentiated human astrocytes displayed two morphotypes, fibrous astrocytes with elongated processes and bushy-to-star-shaped astrocytes that resemble white and gray matter astrocyte morphologies [95] (Figure 3). Under control conditions, both morphotypes displayed calpain activity (blue), but rare and low caspase activity (green). Fetal neocortical cells express calpains 1(μ) and 2(m) along with low endogenous calpain inhibitor calpastatin [96]. Five h post-stretching, injured astrocytes showed blebbing with phase-dark vesicles, vacuoles and beaded processes, known as clasmatodendrosis (Figure 3B,C) [97, 98]. Stretched cultures had a mixed population of astrocytes with leaky and intact plasma membranes documented by variable PI-uptake that suggest dynamic membrane damage and resealing (Figure 3, Additional File1 Figure S10). Acute necrosis with integrity loss were marked by atrophied, phase-dense astrocytes, bright nuclear PI and absence of calpain or caspase activity. Membrane-damaged PI-positive cells had variable caspase and calpain activities depending on morphotype, elongated wounded cells lacked calpain activity while bushy cells were calpain-active (Figure 3B, Additional File1

Figure S10). Caspase activity was detected in cytosol and nuclei of dystrophic cells, and was restricted to nuclei of atrophied cells indicative of ongoing apoptosis (Figure 3C).

Overall, preliminary imaging documents a range of concurrent human astrocyte injury phenotypes and proteolysis states. In the early hours after injury, astrocytes display a spectrum of vulnerability. Enduring trauma states with restoring membrane integrity and proteostasis are important cytoprotective goals that may benefit from monitoring using proteolysis biomarkers including pathological GFAP proteoforms.

Citrullinated GFAP marks a novel trauma-induced CSF signature and astrocyte proteinopathy distinct from classic GFAP

Validated mapping of citrullination and acetylation in GFAP fragments from TBI patients

We analyzed mass spectra for acetylation and citrullination to identify PTM signatures in TBI to support biomarker assay development, and to detect cytoskeleton-destabilizing events and proteinopathies that may impair astrocyte function [43, 99-102]. To our present knowledge, GFAP-PTMs have not been characterized in human TBI patient samples, although GFAP citrullination is observed in chemically stressed cell lines, cell-free systems, and other neurodegenerative diseases [60, 101, 103]. MS-detected acetylated and citrullinated peptide fragments were validated by presence of signature ions and neutral mass losses for four citrullines in coil1 and three in coil2, including a potential novel citrullination site in coil1 (aa R79), which were consistent with observed mass deviations (neutral losses) in MS2 spectra (Figure 4A, Additional File1 Figure S9; Additional File1 Table S4). An additional five here TBI patient detected citrullinations are reported in vitro modifiable GFAP sites citrullinated by PAD treatment [60]. These TBI citrullinations of CSF released GFAP were robust, as they were repeatedly detected and are indicative of GFAP destabilization and pathology [41].

TBI patients have different citrullinated GFAP signatures

Next, citrullination site-specific GFAP antibodies were characterized in human traumatized astrocytes (Additional File1 Figure S10; Additional File1 Table S3) [67]. Two cit-GFAP antibodies with neoepitopes in coil2 gave patient-specific signals distinct from that of classic GFAP (Figure 4B). The most striking was the robust presence of cit-GFAP signals of 13-16kDa and 26-30kDa GFAP-BDPs, not shared by antibodies to unmodified GFAP in same samples. Large GFAP-BDPs were detected by CTGF-1221, as its second epitope (at aa R416) to the uncleaved more c-terminal region was not shared with by cit270-GFAP (detecting aa R270). Additional citrullinated bands above 50kDa are likely pathological GFAP proteoforms, possibly ubiquitinated or multimeric forms [104, 105]. Notably, these patterns had substantial patient-to-patient variation that highlight individual differences in proteolysis and PAD activities during TBI progression and underline the importance of personalized molecular profiling for TBI monitoring.

Citrullinated GFAP in traumatized astrocytes identifies nonfilamentous aggregates

Stretch-trauma cultures had visibly more cit-GFAP signals than controls at 5 and 24h postinjury using Cit270 and two antibodies to classic GFAP (Figure 5, Additional File1 Figure S10). Cit270 stained clusters of small speckles and large granules but did not stain cytoskeletal fibers as shown by GA5 and a polyclonal GFAP antibody. Cit-GFAP aggregates and GFAP filaments were generally not colocalized pending ultrastructural confirmation. Cit-GFAP stained either unmodified GFAP-negative or excessively bright stained cells. Increased GFAP antigenicity is reportedly associated with filament disassembled GFAP after acute wounding, calcium ionophore-treatment, or calpain activation in astrocytes [27, 106]. Morphotypes with cit-GFAP granules included reactive, atrophic (shrunken) and dystrophic astrocytes, named for swollen cell bodies and damaged or missing processes [107]. Cit270 signals were also peppered around astrocyte processes seemingly

extracellular, as phase-contrast images suggest by delineating astrocyte shapes (Figure 5B, Additional File1 Figure S10). Traumatic injury-induced GFAP citrullination and filament breakdown identifies dysfunctional GFAP associated with trauma-burdened human astrocytes.

To conclude, cit-GFAP emerges as a novel trauma marker of an astrocyte proteinopathy in pathological context astrocytes and may aid in individualized TBI patient phenotyping. Together, cit-GFAP detection provides new tools to study astrocyte degeneration and GFAP-driven proteinopathies relevant to the pathophysiology of TBI.

TBI patients' CSF profiles share acute GFAP peaks but differ in fragmentation over time

Temporal trajectory of GFAP degradation after TBI

The average between-experiment CV was 27.8% (n=6 pairs of multiple scaled measurements, specifically 37% for full-length GFAP, 21.5% for fragment bands and 25% for 37kDa band).

age effect shown for GFAP bandsets in Additional File1 Table S6) [72].

Longitudinal GFAP profiles in CSF of 23 Neuro-ICU TBI patients document substantial variability in GFAP- and BDP-band intensities that fluctuated between consecutive samples and across PIDs as immunoblots illustrate (Figure 6A,B). Summated released full-lengths plus fragmented GFAP amounts ("Total" GFAP) also varied among patients as temporal profiles over 10PIDs show ("spaghetti plots", Figure 6C). Typical substrate reaction and exposure saturation limits were overcome by stepwise scaling a dozen exposures that expanded the dynamic range 4-5 orders of magnitude as the span between lower limit of detection and upper limit of quantification document (Additional File1 Table S6). GFAP proteoforms of similar appearance and adjacent sizes were grouped matching pooling of immunoblot and MS data. Age had a significant effect on GFAP release and proteolysis with older patients showing higher CSF levels (Additional File1 Table S7, Additional File1 Figure S13). This reflects both, a known increases in GFAP biofluids in healthy elderly, and altered CSF clearance and a general worse TBI outcome [108, 109]. Total GFAP level peaked on injury day with age adjusted effect size of 1.27 SD units above the weighted mean (p=0.035, Figure 6C) [73]. Full-length GFAP had the highest relative injury day peak with 1.62 SDs above its weighted mean followed by a steady drop (p=0.012, Figure 6D). Mean levels of large GFAP-BDPs decreased sharply over first 2PIDs, then remained flat around their overall mean (p=0.028; Figure 6E). Mean levels of calpain-generated 37-39kDa fragments were highest on injury day with 1.5SDs above their overall mean, stayed elevated on PIDs 2-5 and decreased thereafter (Figure 6F). The two sets of small GFAP-BDPs, 20-26kDa and 15-19kDa, displayed marked dispersion driven by secondary peaks and undetectable values, with greater missingness among 15-19kDa BDPs on later PIDs that produced an injury day peak (1.55 SDs above their weighted mean, Figure 6G,H). Most bands' daily means exceeded the overall mean on until PID4, then fell below on PID7 onward, highlighting a general decline and over time. This general trend suggests ongoing proteolysis seen as decreases in full-length and large GFAP-BDPs, while smaller BDPs had remained elevated or rose on later PIDs. Progressive GFAP clearance from CSF may likely also contribute to this overall temporal biomarker decrease.

Fragment covariation and selective underrepresentation of smallest GFAP-BDPs

Strongest correlation was determined between 50kDa GFAP and calpain-generated 37-39kDa fragments (Pearson coefficient, r=0.82, LogWorth=24.3; Figure 7A, B). The 40-42kDa fragments correlated similarly with the 37-39kDa fragments (r=0.73, LogWorth=16.3). These may reflect co-release and/or general substrate-product relationships. The 15-19kDa BDPs related notably weaker with larger precursors and 20-26kDa coproducts (Figure 7; Additional File1 Figure S14). Specifically, 15–19kDa BDPs had 28% greater missingness than 20–26kDa BDPs across patients (Figure 7C). The lesser covariance -despite their shared cleavage origins- suggests divergent fragment fates. This discrepancy aligns with lower MS coverage, aa

detection frequency and ion peaks of coil2 versus coil1 BDPs in TBI CSF as shown earlier. It is supported by the culture trauma model findings of cell-retained coil2 fragments being prone to cit-modified aggregation. Collectively, these data support a mechanism of selective coil2 retention and preferential coil1 release. This differential accumulation is translationally relevant because linking pathological GFAP proteoforms to biomarker signals has important implications for interpreting GFAP as both a marker of injury and driver of proteinopathy for monitoring and understanding TBI pathophysiology and neurodegeneration as discussed below [110, 111]. Finally, to address the potential of GFAP as marker for injury burden, we evaluated (1) GFAP fragment levels under two severities in culture and (2) the predictive value of GFAP-BDPs for outcome in TBI patients.

GFAP-BDP temporal profiles indicate trauma severity, and predict TBI patient recovery

Time-related calpain GFAP-BDP release associates with trauma severity

To determine the temporal severity relationship between GFAP-BDPs and injury severity, we focused on a fragment present across time points, excluding smaller BDPs previously reported to rise with delayed cell death in traumatized human astrocytes [27]. Release of a 37kDa GFAP fragment was quantified following two stretch severities (3 and 5psi) in astrocytes from 4-9 donors sampled in different batches from 0.5-48h postinjury and in controls (Additional File1 Figure S15). After severe stretching, this fragment was already released early at significant greater levels than in controls and mild stretched samples (0.5-5h, $p<0.05$, Additional File1 Figure S15). At later timepoints fragment levels were elevated over controls in fluids for both severities (24-48h, $p<0.001$). As trendlines illustrate, release increased over time after both severities (0.5h versus 24 and 48h, $p<0.02$, Additional File1 Figure S15B). The proportion of membrane-permeable cells in this trauma model supports these kinetic profiles, additional studies are warranted to address relationships [27]. For the present study, it is reasonable to conclude that the time-course of GFAP cleavage and release may add in evaluating trauma severity.

TBI outcome is predicted by CSF levels of GFAP fragment trajectories but not by those of full-length GFAP

To investigate how GFAP proteolysis relates to patient recovery after TBI, we compared longitudinal CSF levels of full-length GFAP and its fragments in patients with favorable versus unfavorable six-month outcomes via GOSE. Age-controlled CSF means of calpain-generated 37-39kDa GFAP-BDPs distinguished patients with poor outcome (GOSE 1-4) from those with favorable outcome (GOSE 5-8, Cohen's D: 1.1 $p=0.02$; Figure 8, Additional File1 Table S8). Small 20-26kDa BDPs separated good-versus-poor GOSE early postinjury, while adjusted means overlapped during later PIDs. Full-length GFAP levels substantially overlapped across all PIDs. Similar outcome predictions for same GFAP proteoforms were observed using stricter partitioning of favorable outcome (GOSE7+8), indicating the findings were independent of dichotomizing. In summary, longitudinal profiling of GFAP degradation products offers greater prognostic resolution than does full-length GFAP alone and may support early risk stratification and outcome prediction in TBI patients.

In conclusion, TBI triggers GFAP destabilization by citrullination, acetylation and stepwise proteolysis, which are closely associated with astroglial integrity lapses and degeneration. Pathological GFAP aggregation and fragment-specific biofluid profiles are interrelated as novel coproducts emerge from common TBI-GFAP cleavage events that provide new insights for monitoring TBI pathophysiology and recovery prediction.

Limitations

The clinical study had limited sample collection, as it was conducted during the Covid pandemic under substantially short-staffed personnel. Large cohort studies are needed for further covariate inclusion, yet within this study, GFAP band-signals were measured comprehensively in all available samples using subsaturated, calibrated, and scaled quantification. The longitudinal profiling was truncated at 10PIDs to avoid violating unequal variances that forced omitting 3 patients (6 samples) resulting in 23 patients (102 CSF samples). Cohen's D effect size was used to predict good versus poor outcomes, as area-under-the-curve accuracy testing was inadequate for simultaneously including elapsed time postinjury. GFAP band-specific outcome distinction was analyzed for 21 patients (95 samples) as two patients were missing GOSE records. The remaining sample size used omega squared to compute age and temperature effects. Cohen's D effect size was used to predict good versus poor outcomes, as area-under-the-curve accuracy testing was inadequate for simultaneously including elapsed time postinjury. MS sequencing of serum was limited. Ventriculostomy for CSF drainage is employed in 45–80% of severe TBI offering unique biomarker insights for TBI monitoring, yet does carry a small risk of infections [112, 113]. UCLA surgical pathology procurement of donated fetal brain specimen allowed setup of cerebral astrocyte cultures [27, 65], yet primary tissue amounts were limited to cover all relevant conditions simultaneously, yet shown data is representative for other donors. Live-cell staining limited the use of high-intensity illumination or repeated fluorescence imaging but enabled simultaneous monitoring of both enzymes and membrane permeability at a single timepoint. This approach provided insight into coexisting astrocyte injury states, alongside GFAP degradation, modification, and distribution beginning to inform on astrocyte degeneration and TBI monitoring.

Discussion

This study identifies novel TBI-specific GFAP proteolysis as a dynamic process producing proteoforms with distinct patient-specific longitudinal patterns that advance the characterization of postacute TBI progression. Here identified GFAP degradome reveals novel product sets from a common precursor, with surprising divergent fates that link GFAP fluid release to proteinopathy marking pathological astrocytes. Overall, these GFAP-BDP signatures are closely associated with pathological TBI processes driven by perturbed proteostasis.

Cellular and biochemical pathophysiology of mechanical traumatic injury

Mechanical trauma, e.g. whiplash or blunt impact, shears brain microstructures causing diffuse axonal injury and astroglial clasmatodendrosis -membrane wounding that can lead to protracted cell loss [27, 97, 114, 115]. Trauma induces mechanoporation of plasma membranes, triggering rapid release of full-length GFAP and its fragments [27, 116, 117]. High-speed strain stretches intermediate filaments leading to disassembly, rod-domain exposure and susceptibility to proteolysis or even filament breakage [118, 119]. Under biomechanical [41, 106, 120] or may reach a molecular breaking point [119, 121]. Non-filamentous GFAP is documented minutes after stretch-injury in mechanoporated human astrocytes [27]. Thus, filament-disassembly is closely linked to membrane permeability that disturb ion balance and threaten astrocyte viability [27]. Ion imbalance is followed by water influx causing membrane blebbing and astrocyte swelling (oncosis) [122, 123]. If unresolved, and with progressive energy depletion, cell integrity may fail resulting in necrosis. Added stressors such as reactive oxygen species, acidosis and hypoxia further impair mitochondrial function ultimately shifting

cell death pathways from apoptosis to necrosis [122, 124-128]. This progressive pathophysiology unfolds in human astrocytes with considerable delay (unpublished comparison of human and rodent astrocytes). These processes may contribute to secondary GFAP release in TBI patients reflecting cytotoxic edema and subacute astrocyte loss [129-134].

Linking proteases and destabilizing enzymes to GFAP proteinopathy and astrocyte pathology

Assembled GFAP filaments are essential for astrocyte morphology, mechanical resilience, ATP release and other key functions [41]. Calcium ionophore-treated rat astrocytes induces a rapid, transient increase in GFAP immunocytochemical signals due to filament unwinding and epitope exposure [106]. Trauma-induced unfolding may similarly reveal concealed proteolytic cleavage sites within the rod center of GFAP. Calcium influx catalyzes GFAP proteolysis by rapidly activating calpain through conformation change leading to partial GFAP cleavage, consistent with their limited proteolytic activity [41, 106, 116, 135-143]. Calpain cleavage also primes caspase activity hence both enzymes generate small GFAP-BDPs [140, 144]. Calpain activity beyond injury, at baseline is reported and part of the ubiquitin-proteasome, autophagy-lysosomes, and cytoskeleton-remodeling systems, is modulated by inhibitors such as calpastatin and thus consistent with our finding of calpain substrate conversion in unstretched astrocytes [96, 145-147].

Stretch-trauma imposes heterogeneous focal mechanical loading, producing astroglial injury states that vary in severity and progression, further shaped by gray- and white-matter morphotypes with distinct calpain and caspase activities. Caspase activity in process-damaged and blebbing traumatized human astrocytes parallels clasmatodendrosis in excitotoxically injured rat astrocytes linking cytoskeleton remodeling and caspase-mediated breakdown to apoptosis [138, 148]. As cytoskeleton integrity underpins structural resilience and metabolic competence, GFAP proteolysis may exacerbate astrocyte vulnerability as is the case in reduced GFAP expression after injury [117].

Pathological GFAP proteoforms impair astrocyte support function, compromise glutamate buffering and neuronal stability that may lead to neurodegeneration [55]. GFAP destabilization can be driven by calcium-activated PADs, which citrullinate GFAP and other cytoskeleton proteins and is part of GFAP proteinopathy reported in Alexander disease [43, 99-102, 149]. Mechanical stretching, hypoxia and chemical insults induce PADs in astrocytes and Müller glia, consistent with our observation of trauma-driven pathological cit-GFAP formation [104, 150, 151]. Thus, GFAP proteinopathies observed here reflect pathological astrocyte states with potentially harmful consequences. As in Alexander disease, aberrant GFAP critically undermines astrocyte function, jeopardizing neural metabolism, network activity and neurovascular unit integrity [152, 153].

GFAP degradome relevance for GFAP-assays design and interpretation

GFAP testing after TBI is already incorporated into large multisite clinical studies for acute patient assessment using commercial antibody-based platforms [24, 34, 154]. However, beyond a general specificity for GFAP it is not clear what proteoforms are being measured, as this information is typically proprietary or unknown and it is presumed that total released GFAP is captured. The distinct release and modifications of coil1 and coil2 products provide novel insights for design and interpretation of GFAP assays.

Sequences and cleavage of traumatic injury-produced GFAP breakdown products

TBI patient GFAP-BDP sequences display novel cleavage patterns, distinct from established protease sites in other neurodegenerative diseases. A caspase 6 cleavage of GFAP ($VELD_{225}$-VAKP) is described in mouse culture models of Alexander disease, splitting GFAP at the linker2 sequence, with the C-terminal coil2 fragment detected by mab GA5 [54, 66]. We identified longer TBI coil1-products ending 8 or 14 aa beyond

Alexander disease GFAP-BDPs [54]. Hence, a novel TBI-cleavage between residues 240-260 produced these trauma-related GFAP-BDPs. Our MS high confidence peptide maps and MCA5C10 epitope loss ($_{257}$YRSKF$_{261}$) flank a neighboring caspase 3 cleavage site. TBI coil2-products begin at F261 and end at R390 or K410, yet making products shorter than the GFAP-BDPs reported in Alzheimer's disease that are generated by caspase 3 cleavage at $_{258}$RSKFA↓DLTD [83]. While this cleavage can explain the new N-terminus of the coil2-product, it does not explain the shorter coil1-product. Rather, our findings point to coil2A being particularly sensitive to proteolysis after TBI (see below). Our data imply calpain and caspases in this process, though other proteases -including possible endogenous trypsin-like activity ($_{257}$YRSK↓F$_{261}$)- may contribute. Such activity could generate the new termini found in both TBI-GFAP small BDPs (LTAALKEIR↓T; R239) that can account for the observed sequence gap within coil2A between the two product sets. Endogenous trypsin activity is reported after brain injury inflicting astrocyte compromise and adverse inflammatory effects [155, 156]. The gap between the two co-products is unlikely an experimental artifact, as high confidence peptides are repeatedly detected in longer fragments and recombinant GFAP sequences. Further studies are needed to identify additional proteases involved in GFAP cleavage after TBI. The variability in fragment presence and termini suggest different enzymes and fragments could reflect different TBI patient phenotypes.

Structural evidence for protease vulnerability of the novel TBI cleavage site

Intact GFAP molecules anneal by α-helical coiled-coil interactions forming parallel dimers, antiparallel tetramers and ultimately 10nmØ units that grow in length to mature filaments [85]. Computer modeling and structural data show that the entire rod segment of vimentin, closely related to GFAP, is a continuous α-helix [157]. This is despite several regions, historically referred to as linkers or "stutters", lack the typical hydrophobic heptad repeat pattern of α-helical coiled-coils. These regions contain proline and other turn-promoting aa or feature 11aa (hendecad) sequences disrupting the heptad repeats. These regions are therefore thought to represent non-helical linkers. Notably, the Alexander disease-associated cleavage site discussed above is found within one such non-helical regions, "linker12", consisting of several hendecad repeats. Likewise, the region containing the MCA5C10 epitope and caspase3 site are historically referred to as "stutter1", where a hydrophobic heptad repeat (7aa) is replaced by a single hendecad sequence, disrupting the packing and thereby rendering both regions more susceptible to proteases [158].

Pathophysiological significance and biomarker implications of new GFAP-BDPs

TBI proteolysis of GFAP produces coproducts with unequal abundance in patient biofluids with coil1-BDPs being more prevalent than coil2-BDPs in TBI CSF, while the latter are undetected in serum. GFAP concentrations are generally lower in blood versus CSF due to differences in dilution and varied solute passage pathways [53, 159, 160]. The imbalance could reflect differences in release or susceptibility to further degradation. Traumatized astrocytes show preferred coil1-BDP release and selective coil2-BDP retention as non-filamentous cit-GFAP aggregates that mirror toxic Rosenthal fibers of mutant GFAP fragments that impair astrocyte function driving neurodegeneration in Alexander disease [54-56, 66, 161, 162]. Trauma-associated cit-GFAP aggregates are a signature for astrocytopathy and are linked to coproducts in TBI biofluids.

TBI CSF samples carry both coproducts. However, coil2-BDP signals varied -were either missing or elevated- possibly indicating presence or absence of secondary pathological events leading to glial integrity loss with release of otherwise retained proteoforms. Astroglial membrane lysis in necrosis or oncosis during cytotoxic edema are such uncontrolled events [122, 123]. On one hand, coil1-GFAP fluid maybe matched by a latent coil2-GFAP burden in the injured brain. On the other hand, detecting coil2 in fluids may signal worsening conditions such as cytotoxic edema with unregulated astrocyte demise. Thus, coil-specific and cit-GFAP antibodies will serve as pathological astrocyte markers and assay development tools for these secondary TBI

pathologies [42, 98, 163]. These possibilities highlight two priorities for future research of present needs: (1) examine cit-GFAP-aggregates in postmortem TBI, BLAST, or chronic traumatic encephalopathy brains to establish traumatic astrocytopathy as new TBI neuropathological hallmark; and (2) linking GFAP biofluid elevation to proteostasis disruption and neurodegeneration in animal TBI models [18, 111]. Overall, our findings connect GFAP as a TBI fluid biomarker with astroglia proteinopathy and may help track recurring GFAP elevations due to secondary glial deterioration after TBI [27, 29].

Potential for new GFAP 'context of use' in TBI monitoring

Our sequence-defined GFAP degradome linked with cytological data support possible future clinical applications of GFAP in longitudinal TBI patient monitoring. Three interrelated potential COU areas are considered: *(1) Longitudinal monitoring*; (*2) Astrocyte degeneration and secondary injury; (3) Outcome prediction*.

(1) Longitudinal GFAP monitoring and influence of age

Tracking GFAP degradation kinetics offers a longitudinal window for TBI patient monitoring during intensive care and for early clinical trial endpoints [12, 13, 86, 87, 164-167]. GFAP-BDPs dominate in circulation, while CSF carries both, uncleaved GFAP and BDPs [25, 27, 39]. Temporal GFAP profiles with injury day peak (uncleaved and large GFAP-BDPs) are shared with other rapidly degrading TBI biomarkers including UCH-L1, S100β, brain lipid binding protein (BLBP/FABP7), neuron-specific enolase (NSE) and SBDPs [27, 36]. These biomarkers have different half-lives, yet share primary injury-related peaks reflecting on the extent of acute mechanoporation, force-triggered filament breakage and calcium-driven initial proteolysis [19, 27, 28, 168-170].

Secondary to injury-day rise of GFAP-BDPs, particularly of small BDPs with caspase activation, is seen in a subset of TBI patients. This pattern aligns with previous reports of additional later serum GFAP peaks in a subset of older TBI patients with high CT burden, poor outcome, high mortality and pathophysiological features of more severe TBI [29]. Here CSF measured GFAP-BDP levels are also elevated with age. Age-related increases in baseline GFAP and neurofilament light (NfL) relate to reduced clearance or ongoing atrophy [108, 109, 171-173]. Elderly suffering a TBI clear CSF less efficiently through decreased CSF pulsation, ependymal cilia vulnerability, and disrupted cerebral blood flow affecting biomarker levels [174-176]. Upon controlling for age, GFAP and BDPs monitoring can track progressing TBI proteolysis to inform on both initial and secondary TBI pathophysiology (see below).

(2) Detecting astrocyte pathology to inform on secondary injury

Secondary GFAP-BDP elevations appear as patient-specific peaks during injury progression. Neuroimaging reports expanding contusions after TBI, affecting peri-lesional tissue where cytotoxic edema is a major contributor [177-180]. Cytotoxic edema is characterized by microstructural changes of astrocyte swelling and subsequent integrity loss driven by ion dysregulation and metabolic depletion [129-131]. These interrelated mechanisms may underlie the variable secondary increases in cell death-associated BDPs observed in certain TBI patient GFAP trajectories. Consistent with this interpretation, progressive astrocyte degeneration is quantified in autopsied TBI patients' brains with reduced astrocyte numbers between acute (<6h) and subacute (>6hrs to 3PID) postmortem intervals in cerebral white matter and hippocampus [134]. Accordingly, GFAP-BDP profiling has the potential to indicate secondary adverse postinjury events after TBI. Summarizing these two potential COUs, longitudinal GFAP-BDP monitoring in neurocritical care may provide individualized

insights into evolving pathophysiology including discrete secondary adverse events, adding to single-timepoint GFAP testing in the emergency department.

(3) GFAP-BDP trajectories for TBI outcome prediction

Elevated GFAP is recognized as prognostic marker after severe TBI [27, 29, 32, 181-183]. Our findings indicate that it is specifically the timecourse of trauma-generated calpain GFAP-BDPs (37–39kDa) -not uncleaved GFAP or large fragments- that best distinguish poor and good 6-months outcome, regardless of the score partitioning. This dichotomy-robust result is important as defining "good" recovery is inherently personal [184]. The results suggest that ongoing injury-driven GFAP proteolysis offers superior predictive value compared to initial impact-driven uncleaved and end-clipped GFAP levels and aligns with broader clinical knowledge that early injury progression rather than initial status, is what profoundly shapes recovery [185, 186]. Current FDA-approved GFAP testing focuses on a narrow admission window, misses this critical dynamic as longitudinal monitoring is not part of the present COU [31, 181]. Current GFAP assays may include detecting BDPs, yet they don't differentiate between proteoforms, hence don't address degradation. Collectively, serial monitoring of GFAP-BDPs adds value for predicting functional outcomes, because progressive GFAP proteolysis can serve as indicator of disrupted proteostasis during the evolving pathophysiology that shape overall recovery after TBI.

In summary, our findings position GFAP-BDPs as molecular indicators of progressive astrocyte pathology. Trauma-specific GFAP-BDPs and their divergent compartmental fates add mechanistic insight by linking fluid biomarker and latent proteinopathy that can support a new framework for TBI phenotyping, patient monitoring and outcome prognosis.

Acknowledgements

The authors acknowledge with appreciation the receipt of mouse antibody CTGF-1221 to citrullinated GFAP (RRID: AB_3678889) that was kindly provided by Dr. Akihito Ishigami, Tokyo Metropolitan Institute of Gerontology, Tokyo, Japan. Special thanks goes to Dr. Sarah Dry and Ko Kiehle Translational Pathology Core lab, Ronald Reagan UCLA Medical Center, and Dr. Angela Chen, Family Planning & UCLA OBGYN Ronald Reagan Medical Center, for consenting and procuring voluntary donated fetal remains as pre-shelved specimen for cerebral tissues. Greatly appreciates for their grateful for input from are Laboratory assistant Kiohei Itamura, and UCLA Honors students Michelle Gong, Raghu Padmanabhuni, Aryana Sargsyan, Ana Karimi Bidhendi, Emerald Wong, Mhina Cham, Aryana Sargsyan, Kunal Ranat; David Sanville, and for the valuable critical care management assistance provided by Courtney Real and Jesus Ruiz-Tejada and the help from clinical fellow Azim Laiwalla.

Authorship Contributions

IBW conceptualized and designed the study, wrote and revised the manuscript, curated data and conducted formal analysis, designed and prepared all visualizations, acquired funding, coordinated research activities,

supervised laboratory assistants and students and conducted cell culture and live cell imaging studies. **JH** and **JL** conducted sample preparation and immunological experiments, assembled raw data and illustrations, curated and analyzed data. **JL, SS** and **YC** analyzed MS spectra. **YC** and **SS** conducted MS analyses. **HZ** provided the thumbnail infographic. **CS** analyzed data and provided visualizations. **ROL** and **JAL** provided MS data analysis guidance and **JAL** was involved in the study conceptualization. **TVM** and **GS** provided antibodies, peptides and recombinant proteins, assisted in writing the manuscript and offered biochemical guidance. **GS** also conducted antibody binding and chemical cleavage studies and wrote the structural part of the discussion. **BME** provided data interpretation and manuscript revision. **JG** provided guidance on data curation and statistical analysis approaches. **SR** and **PMV** had oversight over clinical aspects of the study including TBI patient enrollment, IRB approval and sample provision. Further, **PMV** provided guidance, manuscript organization and contributed to written content and clinical interpretation of the findings. Resources included **IDDRC** laboratory infrastructure including cell culture, centrifuges, gel imagers. The **MIC** provided mass spectrometry instruments and proteomics facilities for the study. ***All authors*** *read, reviewed, edited and approved of the manuscript.*

Funding

Dana Foundation: Clinical Neuroscience "First in man" award # 20182601: Clinical study and trauma culture model experiments.
Brain Injury Research Center (BIRC), State of California: Clinical study and trauma culture model experiments.
NIH/NINDS Small Business Innovation Research, SBIR grant # 1R43NS106972-01
Validation and GFAP proteoform characterization for assay use
Semel Institute IDDRC and Brain Injury Research Center, BIRC, UCLA, Los Angeles, CA, USA. Facilities and supplies for cell culture and microscopy work.
Sponsored Research Agreement, Abbott Diagnostics: GFAP fragment analyses.
Sponsored Research Agreement, BRAINBox Solutions Inc., Richmond VA, USA: validation studies and patent licensing.

Competing Interest

IBW and **JAL** are inventors of the following patents licensed to BRAINBox Solutions Inc., where **TVM** serves as Chief Scientific Officer (CSO). **GS** is CEO and founder of EnCor Biotechnology Inc., which distributes several monoclonal GFAP antibodies used in this study.
US Patent Issue No.: US 10,557,859 B2 original patent; Inventors I.B. Wanner and J.A. Loo, Issue date: 2/11/2020; 25 claims prior publication 12/20/2018: "Astrocyte traumatome and neurotrauma biomarkers". Applicant Regents of the University of California, Oakland, CA. Licensee: BRAINBox Solutions Inc.
US Issue No.: US 11,249,094 B2 Additional 13 claims in divisional patent 13 Claims, Filed 12/116/2019; Issue date: 2/15/2022; Inventors: Wanner and Loo, UCLA "Astrocyte traumatome and neurotrauma biomarkers". Assignee UCLA; Licensee: Brain Box Solutions Inc.

Additional Material

This manuscript includes a file called Additional File 1 that contains 15 Additional Figure s (labeled Figure s S1-S15) and 8 Additional Tables S1-S8 that are compiled into one ppt file called 'Additional-File1-GFAP trauma-Wanner'.

Data availability

The data master list comprised of de-identified TBI patient clinical variables and outcomes, CSF collection and all GFAP band-specific measurements of the DANA study cohort are uploaded to the Open Data Commons for Traumatic Brain Injury, Wanner lab and is accessible on ODC-TBI with Data dictionary here: https://odc-tbi.org/lab/dataset?labid=387&datasetid=1432

Figure Legends

Thumbnail: Astrocyte injury states with GFAP proteoforms and fates after TBI
The infographic depicts four distinct, progressive -and partially coexisting- pathophysiological states of human astrocytes following TBI. Each injury state is characterized by specific cellular morphologies and GFAP proteoforms and their molecular fates. Illustrated are key processes of GFAP degradation and proteinopathy together with ensuing astrocyte dysfunction that jointly offer a mechanistic basis for longitudinal GFAP fluid biomarker signatures. Understanding these astrocytic and cytoskeletal alterations is central to interpreting GFAP as a TBI biomarker and linking it to neurodegeneration. The thumbnail captures the reasoning for a new GFAP TBI COU in Neuro-ICU patient monitoring and recovery prognostication. **(1) Uninjured***, healthy* astrocyte: Intact processes, continuous plasma membrane and fully assembled GFAP filaments. **(2) Mechanoporated***, wounded* astrocyte: Shear-forces and mechanical loading inflict membrane damage, poration and process beading (clasmatodendrosis), triggering calcium influx and ion imbalance. GFAP filaments get stretched and disassemble into GFAP monomers that may even break (black) and are subsequently degraded, initially by calpains into large fragments (gray BDPs), followed by calpain, caspase and other proteases into novel TBI cleavage co-products: sets of coil1-BDPs (red) and coil2-BDPs (purple). Coil1-BDPs are released into fluids through permeable membranes (red), while coil2-BDPs form intracellular aggregates (purple clusters). **(3) Dystrophic (oncotic),** astrocyte: *Swollen* with vacuoles, membrane blebbing and advanced process damage. Accumulated PTM-modified GFAP granules marked by citrullination (green) and acetylation (brown) represent a GFAP proteinopathy newly recognized in TBI. **(4) Necrotic,** *dying* astrocyte: Loss of membrane integrity, membrane rupture and uncontrolled lysis release modified GFAP aggregates associated with astrocyte demise.

Figure 1: TBI patients' GFAP-BDP sequences display variable product endings

A) TBI patient CSF immunoblots of a 15% gel show GFAP detected by a polyclonal (top) and a monoclonal (clone 3E10, bottom) antibody (postinjury days, i+1 through 1+3) of an 84-year-old male sustaining facial fractures, subarachnoid and intraventricular hemorrhage and intraparenchymal hematomas from a fall. Observed GFAP band molecular weights were bands (II.) 36-39kDa, bands (III.) 20.4-23kDa, and bands (IV.) 17-19kDa, missed by clone 3E10. **B)** MS peptide maps of immunoprecipitated GFAP breakdown products (BDPs) of four cut out gel bandsets (I.-IV., Additional File1 Figure S1) from six CSF TBI samples of three patients. Percent of fragment sequence coverage (left) by high confidence (green, FDR≤1%) and repeatedly identified medium confidence (yellow FDR≤5%) peptides. Bands (I.) had 359 amino acids (aa) with calculated molecular weight of 41.7kDa and suggested new N- and C-termini of serine 53 (S53) and lysine 411 (K411). Bands (II.) spanned 349aa from glycine 56 (G56) to leucine (L404) within which 37/38kDa fragments with variable endings between TBI samples were located (Additional File1 Figure 1). Bands (III.) contained two GFAP-BDPs, 92% covered coil1-containing product of 185aa, calculated molecular weight of 21.8kDa; 77% covered coil2-containing product of 151 aa and peptides, estimated molecular weight of 17.5kDa. Bands (IV.) 96% covered 181 aa coil1 product with size between 21-21.6kDa -±PTMs; and 77% covered coil2 product of 130aa with estimated molecular weight of 15-15.3kDa. **C)** Predicted endings of the two sets of novel TBI patients' GFAP-BDPs. Coil1 products N-termini were S53 (III.) and alanine, A55 (IV.) and new C-termini were arginine 239 (R239) C-terminus (III.) and A233 (IV.), both stretching beyond previously described caspase 6 cleavage around VELD225 [54]. Coil2 products had consistent N-terminus phenylalanine 261 (F261), see reported caspase 3 cleavage RSKFA↓DLTS [83], and variably ended with K411 (III.) and with R390 (IV.).

Figure 2: Novel GFAP cleavage creates co-products with distinct localization fates in TBI

Monoclonal antibody (mab) mapping confirms GFAP cleavage into two co-product sets that resided in separate compartments using a human trauma culture model of in vitro differentiated cerebral astrocytes [65]: coil1-containing products were trauma-released and coil2-products remained cell-associated. **A)** Coil1 or coil2 harboring small GFAP-BDPs for antibody epitope alignment. **B)** Binding regions and defined epitopes of GFAP mabs within coil1 and coil2 GFAP-BDPs. Mab 3E10 binding region is in coil1B between aa 196-217 with stutter motif HEEEVRE, aa204-210, as epitope. Binding region of mab 5C10 covers aa 240-260 in coil 2A with aa257-260 as core epitope. Mab GA5 [54] binds at the end of coil 2B covering aa 374-390. Mouse GFAP multiclone antibody (4A11, 1B4, 2E1 BD Pharmingen) contains unspecified epitopes in both coils. **C)** Two donor's whole cell lysates (Cells) and concentrated media (Fluid) from control (-) and 2 days post-stretched human astrocyte cultures ("+", 4.8-5.4psi) were probed with mab GFAP antibodies. All clones detected full-length GFAP and large fragments in cells and trauma-released fluids. Mab 3E10 detected 20kDa products in fluids but no small BDPs in cells. BD Multiclone detected intracellular 13-28kDa GFAP-BDPs in astrocytes and in extracellular fluids. Mab 5C10 did not detect any small fragments. Mab GA5 [54] detected 17-28kDa GFAP-BDPs in cells, but no small BDPs in fluid.

Figure 3: Inhibition of trauma-induced GFAP degradation across compartments and live imaging of astrocyte injury states show calpain/caspase activation and cell integrity compromises

A) Unstretched or stretch-injured human astrocytes were treated with calpain inhibitor calpeptin (C, 13µM), caspase inhibitor Z-VAD-FMK (V, 11µM), both (CV), or no drug (-) for 48h. Adherent cells were lysed (Whole

Cell lysate, WCL), centrifuged fluid pellet contained lifted material (Lifted Cell Pellet) and fluids were concentrated (Conditioned medium, CM). *Top:* 2s exposures for 50kDa GFAP and 42-47kDa BDPs. *Mid:* 1min exposures for 38-25kDa BDP bands. *Bottom:* 20min (WCL, CM) and 5min (Lifted cell pellet) exposures for 17-25kDa BDPs (See Additional File1 Figure S7). **B+C)** *Live imaging of distinct cerebral human astrocyte morphotypes and their acute trauma stages defined by membrane leak, calpain and caspase activities during 5-6 hours postinjury.* **B)**. *Left*: Elongated (*Top*) and bushy (*bottom*) morphotypes and injury shapes on phase contrast. *Right*: Fluorescence images for plasma membrane permeability (5min uptake assay of propidium iodide, [PI+], red), calpain activity (CMAC-tBOC-leucyl-methionine, [CMAC-tBLM], converted substrate, blue) and caspase activity ([NucView488] converted substrate, green). *Top*: Control fibrous astrocytes display intact processes, acutely stretched cells had thinned, frequently beaded clasmatodendrotic processes (arrows). [PI-] astrocytes were calpain active. [PI+], leaky cells presented variable caspase activity (yellow/orange), lacking calpain-activity. *Bottom*: Bushy control and stretched astrocytes were calpain active (blue). The majority of stretched bushy astrocytes were calpain and caspase active (teal). [PI+], leaky bushy cells either retained both activities (yellow/white), or lost these protease activities (red, arrows) displaying necrotic, atrophic morphology. Phase-dense vacuoles were unstained. See Additional File1 Figure S8 for separate fluorescence channels. **C)** Enlarged from B: Individual fibrous (top) and bushy (bottom) astrocytes showing distinct structural and functional features of intact, injured and necrotic astrocyte phenotypes: *Intact* [PI-], calpain [+]; *Wounded*: [PI-/+], cytoplasmic and nuclear caspase [+]; *Dying:* [PI+] nuclear caspase [-/+], calpain [-]. Scale bars: 100 µm.

Figure 4: Destabilizing citrullination and acetylation PTMs are signatures of TBI patients' GFAP

A) Map shows GFAP coil1/2-BDPs with posttranslationally modified aa from MS of six TBI CSF samples. Citrullinations (green) included a novel citrullination site at arginine 188 (R188), and acetylations (brown) PTMs were validated by signature ions and ion mass shifts in MS2 spectra (Additional File1 Figure S6). *Here identified citrullinations are prior described in cell-free peptidylarginine deiminase digests [60]. Arrows: Neo-epitopes R270 and R416 for citrullinated-GFAP specific antibodies cit-R270-GFAP, mab CTGF-1221 [67] used in B and Figure 5. **B)** *Left*: TBI patient-specific citrullinated GFAP-BDP signatures in nine CSF samples from five TBI patients using two cit-GFAP antibodies. Besides fragments, larger modified GFAP bands were present. *Right*: Unmodified GFAP detected by cloil1 mab3E10 (top) or a rabbit polyclonal GFAP (bottom) show different signal patterns and amounts as cit-GFAP on same samples (dilutions and exposures see Additional File1 Table S3).

Figure 5: Trauma induced citrullinated GFAP formed aggregated clusters in pathological human astrocytes

A) Immunofluorescence of coil2 GFAP (mabGA5, red) and citrullinated GFAP (cit270-GFAP, green) shows trauma-enhanced accumulation of non-filamentous citrullinated GFAP clusters at 5 and 24h post-stretching (right) versus control astrocytes (left) astrocytes. **B)** Unstretched astrocyte (left) and three trauma-pathological astrocyte morphotypes (right) after stretch-injury: reactive astrocyte with thick, hypertrophied processes and bright GFAP with somatic fine-granular cit-GFAP (yellow); astrocytes with fanning-out processes display cit-GFAP sprinkles around GA5 signals (arrows); dystrophic, oncotic astrocytes with swollen somata and malformed or missing processes display non-filamentous GFAP and cit-GFAP aggregates (arrowheads; Additional File1 Figure S10 for sole cit-GFAP signals and polyclonal GFAP signals, E for cell borders). Scale bars: 50 µm.

Figure 6: TBI patient longitudinal CSF GFAP size-specific patterns display common acute GFAP peaks, individual secondary GFAP profiles and unique GFAP degradation profiles

A) GFAP immunoblot of 16 serial CSF samples over four postinjury days from a 40-year-old white male TBI patients with admission GCS 3 and good recovery (GOSE score 8). Strongest GFAP and fragment signals were six hours postinjury and secondary peaks of GFAP (37-50kDa) occurred on PID2-4. **B)** GFAP immunoblot shows seven serial CSF samples from PID4-10 of a 48-year-old Hispanic male TBI patient with admission GCS10 and GOSE6 outcome. Bands 37-50kDa were stronger on earlier days while 15-26kDa BDPs variably increased on PID5-8. **C-H:** *TBI patients' 10PID longitudinal profiles of GFAP total* ***(C),*** *uncleaved* ***(D)*** *and degradation BDP sets* ***(E-H).*** Graphed are log-transformed GFAP CSF trajectories measured on repeated exposures of subsaturated scaled and calibrated (colored lines; 102 observations, 23 TBI patients; densitometry approach see Additional File1 Figure S11; Additional File1 Table S5). Added are variance-weighted Cohen's D effect size, estimated resampled mean cubic splines with 95% CI bounds, interquartile range (IQR, log ng/ml), kurtosis and variance (σ: log(ng/ml)^2). **D, E, H)** Total, full-length GFAP, large GFAP-BDPs and 15-19kDa small GFAP-BDPs were significantly higher on injury day than on other PIDs ($p<0.05$; Linear mixed model, controlling for age, Additional File1 Table S7, Additional File1 Figure S13). 15-19kDa BDPs had large dispersion due to high or undetected bands (difference to other proteoforms see I, K). **F)** Calpain-generated 37-39kDa GFAP fragments trended high on injury day and displayed above mean signals until PID3, around mean signals on PID4 and 5 and below mean signals thereafter. **G)** Small GFAP-BDPs sized 20-26kDa had pronounced secondary highs and largest dispersion (highest IQR, variance and kurtosis).

Figure 7: Correlation between sets of GFAP proteoforms in TBI patients' CSF

A) Multivariate Pearson's correlation matrix shows correlation coefficients between uncleaved GFAP and all BDP sets measured in same TBI CSF samples. **B)** Bivariate graph of full length (50kDa) GFAP over calpain cleavage products (37-39kDa) with orthogonal fit for equal error weights, R^2 and FDR-corrected Logworth ($\log_{10}$p-values, false discovery rate corrected). **C)** Bivariate graph of GFAP-BDP co-products show greater missingness among 15-19kDa versus 20-26kDa bandsets (circled, 28% or 15 more zeroes; orthogonal fit, FDR-corrected Logworth).

Figure 8: Dynamic GFAP proteolysis differentiates poor from good TBI patient outcome not full-length GFAP profiles

Shown are trajectories of GFAP molecular weights over 10PIDs partitioned by good recovery (GOSE 5-8) versus poor outcome (GOSE1-4) with mean cubic splines and 95% CI bands (21 patients; 95 observations). **A)** Calpain generated 37-39kDa GFAP-BDP trajectories differed in outcome by 1.1SD unit ($p=0.02$, Cohen's D adjusted for elapsed time and age effects; subject ID as random effect). **B)** Small GFAP-BDPs (20-26kDa) showed 0.9SD mean higher levels in patients with poor recovery over time than those with good recovery with trends influenced by age and missingness. **C)** Full-length, 50kDa GFAP profiles overlapped over time lacking differentiation between good versus poor outcome. **D)** GFAP means adjusted for elapsed time postinjury and age are graphed between poor and good outcomes showing linear mixed model results.

References

1. Maas AIR, Menon DK, Manley GT, Abrams M, Åkerlund C, Andelic N, et al. Traumatic brain injury: progress and challenges in prevention, clinical care, and research. The Lancet Neurology. 2022;21(11):1004-60.doi:https://doi.org/10.1016/S1474-4422(22)00309-X
2. Karamian A, Lucke-Wold B, Seifi A. Prevalence of Traumatic Brain Injury in the General Adult Population of the USA: A Meta-Analysis. Neuroepidemiology. 2024:1-10.doi:10.1159/000540676
3. Nelson LD, Temkin NR, Barber J, Brett BL, Okonkwo DO, McCrea MA, et al. Functional Recovery, Symptoms, and Quality of Life 1 to 5 Years After Traumatic Brain Injury: Findings From the TRACK-TBI Study. JAMA Network Open. 2023;6(3):e233660-e.doi:10.1001/jamanetworkopen.2023.3660
4. Nelson LD, Temkin NR, Dikmen S, Barber J, Giacino JT, Yuh E, et al. Recovery After Mild Traumatic Brain Injury in Patients Presenting to US Level I Trauma Centers: A Transforming Research and Clinical Knowledge in Traumatic Brain Injury (TRACK-TBI) Study. JAMA neurology. 2019.doi:10.1001/jamaneurol.2019.1313
5. Mavroudis I, Kazis D, Petridis FE, Balmus IM, Papaliagkas V, Ciobica A. The Association Between Traumatic Brain Injury and the Risk of Cognitive Decline: An Umbrella Systematic Review and Meta-Analysis. Brain Sci. 2024;14(12).doi:10.3390/brainsci14121188
6. Shin MK, Vazquez-Rosa E, Koh Y, Dhar M, Chaubey K, Cintron-Perez CJ, et al. Reducing acetylated tau is neuroprotective in brain injury. Cell. 2021;184(10):2715-32 e23.doi:10.1016/j.cell.2021.03.032
7. Brett BL, Gardner RC, Godbout J, Dams-O'Connor K, Keene CD. Traumatic Brain Injury and Risk of Neurodegenerative Disorder. Biological psychiatry. 2022;91(5):498-507.doi:10.1016/j.biopsych.2021.05.025
8. Quinn JP, Corbett NJ, Kellett KAB, Hooper NM. Tau Proteolysis in the Pathogenesis of Tauopathies: Neurotoxic Fragments and Novel Biomarkers. Journal of Alzheimer's Disease. 2018;63(1):13-33.doi:10.3233/jad-170959
9. Gupta R, Sahu M, Srivastava D, Tiwari S, Ambasta RK, Kumar P. Post-translational modifications: Regulators of neurodegenerative proteinopathies. Ageing Res Rev. 2021;68:101336.doi:10.1016/j.arr.2021.101336
10. Xia Y, Lloyd GM, Giasson BI. Targeted proteolytic products of τ and α-synuclein in neurodegeneration. Essays Biochem. 2021;65(7):905-12.doi:10.1042/ebc20210028
11. Deng Y, Thompson BM, Gao X, Hall ED. Temporal relationship of peroxynitrite-induced oxidative damage, calpain-mediated cytoskeletal degradation and neurodegeneration after traumatic brain injury. Experimental neurology. 2007;205(1):154-65.doi:10.1016/j.expneurol.2007.01.023
12. Saatman KE, Creed J, Raghupathi R. Calpain as a Therapeutic Target in Traumatic Brain Injury. Neurotherapeutics : the journal of the American Society for Experimental NeuroTherapeutics. 2010;7(1):31-42.doi:https://doi.org/10.1016/j.nurt.2009.11.002
13. Zhang A, Zhang Z, Liu Y, Lenahan C, Xu H, Jiang J, et al. The Role of Caspase Family in Acute Brain Injury: The Potential Therapeutic Targets in the Future. Current neuropharmacology. 2022;20(6):1194-211.doi:10.2174/1570159x19666211111121146
14. Baudry M, Bi X. Calpain-1 and Calpain-2: The Yin and Yang of Synaptic Plasticity and Neurodegeneration. Trends Neurosci. 2016;39(4):235
15. Beer R, Franz G, Srinivasan A, Hayes RL, Pike BR, Newcomb JK, et al. Temporal profile and cell subtype distribution of activated caspase-3 following experimental traumatic brain injury. Journal of neurochemistry. 2000;75(3):1264-73
16. Ng SY, Lee AYW. Traumatic Brain Injuries: Pathophysiology and Potential Therapeutic Targets. Frontiers in Cellular Neuroscience. 2019;Volume 13 - 2019.doi:10.3389/fncel.2019.00528

17. Giza CC, Hovda DA. The new neurometabolic cascade of concussion. Neurosurgery. 2014;75 Additional File1 4:S24-33.doi:10.1227/NEU.0000000000000505
18. Pereira JB, Janelidze S, Smith R, Mattsson-Carlgren N, Palmqvist S, Teunissen CE, et al. Plasma GFAP is an early marker of amyloid-β but not tau pathology in Alzheimer's disease. Brain : a journal of neurology. 2021;144(11):3505-16.doi:10.1093/brain/awab223
19. Pineda JA, Lewis SB, Valadka AB, Papa L, Hannay HJ, Heaton SC, et al. Clinical significance of alphaII-spectrin breakdown products in cerebrospinal fluid after severe traumatic brain injury. Journal of neurotrauma. 2007;24(2):354-66.doi:10.1089/neu.2006.003789
20. Ringger NC, O'Steen BE, Brabham JG, Silver X, Pineda J, Wang KK, et al. A novel marker for traumatic brain injury: CSF alphaII-spectrin breakdown product levels. Journal of neurotrauma. 2004;21(10):1443-56
21. Stankewich MC, Cianci CD, Stabach PR, Ji L, Nath A, Morrow JS. Cell organization, growth, and neural and cardiac development require αII-spectrin. Journal of cell science. 2011;124(23):3956-66.doi:10.1242/jcs.080374
22. Machnicka B, Ponceau A, Picot J, Colin Y, Lecomte MC. Deficiency of αII-spectrin affects endothelial cell-matrix contact and migration leading to impairment of angiogenesis in vitro. Cell Mol Biol Lett. 2020;25:3.doi:10.1186/s11658-020-0200-y
23. Metting Z, Wilczak N, Rodiger LA, Schaaf JM, van der Naalt J. GFAP and S100B in the acute phase of mild traumatic brain injury. Neurology. 2012;78(18):1428-33.doi:10.1212/WNL.0b013e318253d5c7
24. Bazarian JJ, Biberthaler P, Welch RD, Lewis LM, Barzo P, Bogner-Flatz V, et al. Serum GFAP and UCH-L1 for prediction of absence of intracranial injuries on head CT (ALERT-TBI): a multicentre observational study. The Lancet Neurology. 2018;17(9):782-9.doi:10.1016/S1474-4422(18)30231-X
25. Papa L, Lewis LM, Falk JL, Zhang Z, Silvestri S, Giordano P, et al. Elevated levels of serum glial fibrillary acidic protein breakdown products in mild and moderate traumatic brain injury are associated with intracranial lesions and neurosurgical intervention. Annals of emergency medicine. 2012;59(6):471-83.doi:10.1016/j.annemergmed.2011.08.021
26. Papa L, McKinley WI, Valadka AB, Newman ZC, Nordgren RK, Pramuka PE, et al. Diagnostic Performance of GFAP, UCH-L1, and MAP-2 Within 30 and 60 Minutes of Traumatic Brain Injury. JAMA Network Open. 2024;7(9):e2431115-e.doi:10.1001/jamanetworkopen.2024.31115
27. Halford J, Shen S, Itamura K, Levine J, Chong AC, Czerwieniec G, et al. New astroglial injury-defined biomarkers for neurotrauma assessment. Journal of cerebral blood flow and metabolism : official journal of the International Society of Cerebral Blood Flow and Metabolism. 2017;37(10):3278-99.doi:10.1177/0271678X17724681
28. Papa L, Brophy GM, Welch RD, Lewis LM, Braga CF, Tan CN, et al. Time Course and Diagnostic Accuracy of Glial and Neuronal Blood Biomarkers GFAP and UCH-L1 in a Large Cohort of Trauma Patients With and Without Mild Traumatic Brain Injury. JAMA neurology. 2016;73(5):551-60.doi:10.1001/jamaneurol.2016.0039
29. Robertson CS, Martinez FS, McQuillan LE, Williamson J, Lamb DG, Wang KKW, et al. Serial Measurements of Serum Glial Fibrillary Acidic Protein in Moderate-Severe Traumatic Brain Injury: Potential Utility in Providing Insights into Secondary Insults and Long-Term Outcome. Journal of neurotrauma. 2024;41(1-2):73-90.doi:10.1089/neu.2023.0111
30. Lumpkins KM, Bochicchio GV, Keledjian K, Simard JM, McCunn M, Scalea T. Glial fibrillary acidic protein is highly correlated with brain injury. The Journal of trauma. 2008;65(4):778-82; discussion 82-4
31. Wilson L, Newcombe VFJ, Whitehouse DP, Mondello S, Maas AIR, Menon DK, et al. Association of early blood-based biomarkers and six-month functional outcomes in conventional severity categories of traumatic brain injury: capturing the continuous spectrum of injury. eBioMedicine. 2024;107.doi:10.1016/j.ebiom.2024.105298

32. Pelinka LE, Kroepfl A, Leixnering M, Buchinger W, Raabe A, Redl H. GFAP versus S100B in serum after traumatic brain injury: relationship to brain damage and outcome. Journal of neurotrauma. 2004;21(11):1553-61
33. Okonkwo DO, Puffer RC, Puccio AM, Yuh EL, Yue JK, Diaz-Arrastia R, et al. Point-of-Care Platform Blood Biomarker Testing of Glial Fibrillary Acidic Protein versus S100 Calcium-Binding Protein B for Prediction of Traumatic Brain Injuries: A Transforming Research and Clinical Knowledge in Traumatic Brain Injury Study. Journal of neurotrauma. 2020;37(23):2460-7.doi:10.1089/neu.2020.7140
34. Bazarian JJ, Zetterberg H, Buki A, Dengler BA, Diaz-Arrastia R, Korley FK, et al. Blood-Based Biomarkers for Improved Characterization of Traumatic Brain Injury: Recommendations from the 2024 National Institute for Neurological Disorders and Stroke Traumatic Brain Injury Classification and Nomenclature Initiative Blood-Based Biomarkers Working Group. Journal of neurotrauma. 2025.doi:10.1089/neu.2024.0581
35. Manley GT, Dams-O'Connor K, Alosco ML, Awwad HO, Bazarian JJ, Bragge P, et al. A new characterisation of acute traumatic brain injury: the NIH-NINDS TBI Classification and Nomenclature Initiative. The Lancet Neurology. 2025;24(6):512-23.doi:10.1016/S1474-4422(25)00154-1
36. Wilde EA, Wanner IB, Kenney K, Gill J, Stone JR, Disner S, et al. A Framework to Advance Biomarker Development in the Diagnosis, Outcome Prediction, and Treatment of Traumatic Brain Injury. Journal of neurotrauma. 2022;39(7-8):436-57.doi:10.1089/neu.2021.0099
37. Diaz-Arrastia R. Performance of Diagnostic Biomarkers for Traumatic Brain Injury Within the First Hour-Expanding Their Clinical Utility. JAMA Netw Open. 2024;7(9):e2431102.doi:10.1001/jamanetworkopen.2024.31102
38. Thelin EP, Zeiler FA, Ercole A, Mondello S, Buki A, Bellander BM, et al. Serial Sampling of Serum Protein Biomarkers for Monitoring Human Traumatic Brain Injury Dynamics: A Systematic Review. Frontiers in neurology. 2017;8:300.doi:10.3389/fneur.2017.00300
39. Zoltewicz JS, Mondello S, Yang B, Newsom KJ, Kobeissy F, Yao C, et al. Biomarkers track damage after graded injury severity in a rat model of penetrating brain injury. Journal of neurotrauma. 2013;30(13):1161-9.doi:10.1089/neu.2012.2762
40. McMahon PJ, Panczykowski DM, Yue JK, Puccio AM, Inoue T, Sorani MD, et al. Measurement of the glial fibrillary acidic protein and its breakdown products GFAP-BDP biomarker for the detection of traumatic brain injury compared to computed tomography and magnetic resonance imaging. Journal of neurotrauma. 2015;32(8):527-33.doi:10.1089/neu.2014.3635
41. Phillips CL, Faridounnia M, Armao D, Snider NT. Stability dynamics of neurofilament and GFAP networks and protein fragments. Current opinion in cell biology. 2023;85:102266.doi:10.1016/j.ceb.2023.102266
42. Sofroniew MV, Vinters HV. Astrocytes: biology and pathology. Acta Neuropathol. 2010;119(1):7-35
43. Messing A, Brenner M. GFAP at 50. ASN neuro. 2020;12:1759091420949680.doi:10.1177/1759091420949680
44. Hinkle DA, Baldwin SA, Scheff SW, Wise PM. GFAP and S100beta expression in the cortex and hippocampus in response to mild cortical contusion. Journal of neurotrauma. 1997;14(10):729-38
45. Lin NH, Jian WS, Snider N, Perng MD. Glial fibrillary acidic protein is pathologically modified in Alexander disease. The Journal of biological chemistry. 2024;300(7):107402.doi:10.1016/j.jbc.2024.107402
46. Olabarria M, Goldman JE. Disorders of Astrocytes: Alexander Disease as a Model. Annual Review of Pathology: Mechanisms of Disease. 2017;12(Volume 12, 2017):131-52.doi:https://doi.org/10.1146/annurev-pathol-052016-100218
47. Muñoz-Ballester C, Robel S. Astrocyte-mediated mechanisms contribute to traumatic brain injury pathology. WIREs Mech Dis. 2023;15(5):e1622.doi:10.1002/wsbm.1622
48. Zhao X, Ahram A, Berman RF, Muizelaar JP, Lyeth BG. Early loss of astrocytes after experimental traumatic brain injury. Glia. 2003;44(2):140-52.doi:10.1002/glia.10283

49. Pajares MA, Hernández-Gerez E, Pekny M, Pérez-Sala D. Alexander disease: the road ahead. Neural Regen Res. 2023;18(10):2156-60.doi:10.4103/1673-5374.369097
50. Messing A, Goldman JE, Johnson AB, Brenner M. Alexander Disease: New Insights From Genetics. Journal of Neuropathology & Experimental Neurology. 2001;60(6):563-73.doi:10.1093/jnen/60.6.563
51. Heaven MR, Flint D, Randall SM, Sosunov AA, Wilson L, Barnes S, et al. Composition of Rosenthal Fibers, the Protein Aggregate Hallmark of Alexander Disease. Journal of proteome research. 2016;15(7):2265-82.doi:10.1021/acs.jproteome.6b00316
52. Ashton NJ, Di Molfetta G, Tan K, Blennow K, Zetterberg H, Messing A. Plasma concentrations of glial fibrillary acidic protein, neurofilament light, and tau in Alexander disease. Neurol Sci. 2024;45(9):4513-8.doi:10.1007/s10072-024-07495-8
53. Jany PL, Agosta GE, Benko WS, Eickhoff JC, Keller SR, Köehler W, et al. CSF and Blood Levels of GFAP in Alexander Disease. eneuro. 2015;2(5):ENEURO.0080-15.2015.doi:10.1523/eneuro.0080-15.2015
54. Chen MH, Hagemann TL, Quinlan RA, Messing A, Perng MD. Caspase cleavage of GFAP produces an assembly-compromised proteolytic fragment that promotes filament aggregation. ASN neuro. 2013;5(5):e00125.doi:10.1042/AN20130032
55. Lin NH, Yang AW, Chang CH, Perng MD. Elevated GFAP isoform expression promotes protein aggregation and compromises astrocyte function. FASEB journal : official publication of the Federation of American Societies for Experimental Biology. 2021;35(5):e21614.doi:10.1096/fj.202100087R
56. Der Perng M, Su M, Wen SF, Li R, Gibbon T, Prescott AR, et al. The Alexander disease-causing glial fibrillary acidic protein mutant, R416W, accumulates into Rosenthal fibers by a pathway that involves filament aggregation and the association of alpha B-crystallin and HSP27. Am J Hum Genet. 2006;79(2):197-213.doi:10.1086/504411
57. Chen W, Nishikimi A, Kamata T, Adachi Y. A reducing and denaturing step maximizes the immunoprecipitations of m-calpain and I-2(PP2A)/SET: an approach toward antibodies that do not work well in immunoprecipitation. J Biochem Biophys Methods. 2006;68(1):65-8.doi:10.1016/j.jbbm.2006.02.012
58. Michielsen EC, Diris JH, Hackeng CM, Wodzig WK, Van Dieijen-Visser MP. Highly sensitive immunoprecipitation method for extracting and concentrating low-abundance proteins from human serum. Clinical chemistry. 2005;51(1):222-4.doi:10.1373/clinchem.2004.036251
59. Bons JA, Michielsen EC, de Boer D, Bouwman FG, Jaeken J, van Dieijen-Visser MP, et al. A specific immunoprecipitation method for isolating isoforms of insulin-like growth factor binding protein-3 from serum. Clin Chim Acta. 2008;387(1-2):59-65.doi:10.1016/j.cca.2007.09.002
60. Jin Z, Fu Z, Yang J, Troncosco J, Everett AD, Van Eyk JE. Identification and characterization of citrulline-modified brain proteins by combining HCD and CID fragmentation. Proteomics. 2013;13(17):2682-91.doi:10.1002/pmic.201300064
61. Han K-K, Richard C, Biserte G. Current developments in chemical cleavage of proteins. International Journal of Biochemistry. 1983;15(7):875-84.doi:https://doi.org/10.1016/0020-711X(83)90162-3
62. Vestling MM, Kelly MA, Fenselau C. Optimization by mass spectrometry of a tryptophan-specific protein cleavage reaction. Rapid Commun Mass Spectrom. 1994;8(9):786-90.doi:10.1002/rcm.1290080925
63. Kouklis PD, Traub P, Georgatos SD. Involvement of the consensus sequence motif at coil 2b in the assembly and stability of vimentin filaments. Journal of cell science. 1992;102 (Pt 1):31-41.doi:10.1242/jcs.102.1.31
64. Pruss RM. Efficient detection of intermediate filament proteins using a panspecific monoclonal antibody: anti-IFA. Journal of neuroimmunology. 1985;8(4-6):293-9.doi:10.1016/s0165-5728(85)80068-0
65. Wanner IB. An in vitro trauma model to study rodent and human astrocyte reactivity. Methods in molecular biology. 2012;814:189-219.doi:10.1007/978-1-61779-452-0_14
66. Chen YS, Lim SC, Chen MH, Quinlan RA, Perng MD. Alexander disease causing mutations in the C-terminal domain of GFAP are deleterious both to assembly and network formation with the potential to both

activate caspase 3 and decrease cell viability. Exp Cell Res. 2011;317(16):2252-66.doi:10.1016/j.yexcr.2011.06.017
67. Ishigami A, Masutomi H, Handa S, Nakamura M, Nakaya S, Uchida Y, et al. Mass spectrometric identification of citrullination sites and immunohistochemical detection of citrullinated glial fibrillary acidic protein in Alzheimer's disease brains. Journal of neuroscience research. 2015;93(11):1664-74.doi:10.1002/jnr.23620
68. Lee MS, Kwon YT, Li M, Peng J, Friedlander RM, Tsai LH. Neurotoxicity induces cleavage of p35 to p25 by calpain. Nature. 2000;405(6784):360-4.doi:10.1038/35012636
69. Yap YW, Whiteman M, Bay BH, Li Y, Sheu FS, Qi RZ, et al. Hypochlorous acid induces apoptosis of cultured cortical neurons through activation of calpains and rupture of lysosomes. Journal of neurochemistry. 2006;98(5):1597-609.doi:10.1111/j.1471-4159.2006.03996.x
70. Ekert PG, Silke J, Vaux DL. Caspase inhibitors. Cell death and differentiation. 1999;6(11):1081-6.doi:10.1038/sj.cdd.4400594
71. Knoblach SM, Alroy DA, Nikolaeva M, Cernak I, Stoica BA, Faden AI. Caspase inhibitor z-DEVD-fmk attenuates calpain and necrotic cell death in vitro and after traumatic brain injury. Journal of cerebral blood flow and metabolism : official journal of the International Society of Cerebral Blood Flow and Metabolism. 2004;24(10):1119-32.doi:10.1097/01.WCB.0000138664.17682.32
72. Kroes ADA, Finley JR. Demystifying omega squared: Practical guidance for effect size in common analysis of variance designs. Psychol Methods. 2023.doi:10.1037/met0000581
73. Nelson PR, Wludyka PS, Copeland KAF. Analysis of Means: A Graphical Method for Comparing Means, Rates and Proportions. Asa Siam Ser Stat Ap. 2005;18:1-247.doi:10.1137/1.9780898718362
74. Hsu JC, Nelson B. Multiple comparisons in the general linear model. J Comput Graph Stat. 1998;7(1):23-41.doi:Doi 10.2307/1390767
75. Lakens D. Calculating and reporting effect sizes to facilitate cumulative science: a practical primer for t-tests and ANOVAs. Frontiers in Psychology. 2013;4.doi:10.3389/fpsyg.2013.00863
76. Lakshmi R, Sajesh TA. A robust distance-based approach for detecting multidimensional outliers. J Appl Stat. 2025;52(6):1278-98.doi:10.1080/02664763.2024.2422403
77. Van Aelst S, Van Driessen K, Rousseeuw PJ. A robust method for multivariate regression. St Class Dat Anal. 2000:309-14
78. Habshah M, Sani M, Arasan J. Robust Heteroscedasticity Consistent Covariance Matrix Estimator based on Robust Mahalanobis Distance and Diagnostic Robust Generalized Potential Weighting Methods in Linear Regression. J Mod Appl Stat Meth. 2018;17(1).doi:ARTN 17 10.22237/jmasm/1530279855
79. Shi Y, Mowery RA, Ashley J, Hentz M, Ramirez AJ, Bilgicer B, et al. Abnormal SDS-PAGE migration of cytosolic proteins can identify domains and mechanisms that control surfactant binding. Protein Sci. 2012;21(8):1197-209.doi:10.1002/pro.2107
80. Guan Y, Zhu Q, Huang D, Zhao S, Jan Lo L, Peng J. An equation to estimate the difference between theoretically predicted and SDS PAGE-displayed molecular weights for an acidic peptide. Scientific reports. 2015;5:13370.doi:10.1038/srep13370
81. Inagaki M, Nakamura Y, Takeda M, Nishimura T, Inagaki N. Glial fibrillary acidic protein: dynamic property and regulation by phosphorylation. Brain pathology. 1994;4(3):239-43.doi:10.1111/j.1750-3639.1994.tb00839.x
82. Boyd SE, Nair B, Ng SW, Keith JM, Orian JM. Computational Characterization of 3′ Splice Variants in the GFAP Isoform Family. PloS one. 2012;7(3):e33565.doi:10.1371/journal.pone.0033565
83. Mouser PE, Head E, Ha KH, Rohn TT. Caspase-mediated cleavage of glial fibrillary acidic protein within degenerating astrocytes of the Alzheimer's disease brain. The American journal of pathology. 2006;168(3):936-46.doi:10.2353/ajpath.2006.050798

84. Yang Z, Arja RD, Zhu T, Sarkis GA, Patterson RL, Romo P, et al. Characterization of Calpain and Caspase-6-Generated Glial Fibrillary Acidic Protein Breakdown Products Following Traumatic Brain Injury and Astroglial Cell Injury. International Journal of Molecular Sciences. 2022;23(16):8960
85. Kim B, Kim S, Jin MS. Crystal structure of the human glial fibrillary acidic protein 1B domain. Biochemical and biophysical research communications. 2018;503(4):2899-905.doi:10.1016/j.bbrc.2018.08.066
86. Knoblach SM, Nikolaeva M, Huang X, Fan L, Krajewski S, Reed JC, et al. Multiple caspases are activated after traumatic brain injury: evidence for involvement in functional outcome. Journal of neurotrauma. 2002;19(10):1155-70.doi:10.1089/08977150260337967
87. Baudry M, Luo YL, Bi X. Calpain-2 Inhibitors as Therapy for Traumatic Brain Injury. Neurotherapeutics : the journal of the American Society for Experimental NeuroTherapeutics. 2023;20(6):1592-602.doi:10.1007/s13311-023-01407-y
88. Dhani S, Zhao Y, Zhivotovsky B. A long way to go: caspase inhibitors in clinical use. Cell Death & Disease. 2021;12(10):949.doi:10.1038/s41419-021-04240-3
89. Liu MC, Akle V, Zheng W, Dave JR, Tortella FC, Hayes RL, et al. Comparing calpain- and caspase-3-mediated degradation patterns in traumatic brain injury by differential proteome analysis. The Biochemical journal. 2006;394(Pt 3):715-25
90. Kim JH, Kwon SJ, Stankewich MC, Huh GY, Glantz SB, Morrow JS. Reactive protoplasmic and fibrous astrocytes contain high levels of calpain-cleaved alpha 2 spectrin. Exp Mol Pathol. 2016;100(1):1-7.doi:10.1016/j.yexmp.2015.11.005
91. Roberts-Lewis JM, Savage MJ, Marcy VR, Pinsker LR, Siman R. Immunolocalization of calpain I-mediated spectrin degradation to vulnerable neurons in the ischemic gerbil brain. The Journal of neuroscience : the official journal of the Society for Neuroscience. 1994;14(6):3934-44
92. Siman R, Shahim P, Tegner Y, Blennow K, Zetterberg H, Smith DH. Serum SNTF Increases in Concussed Professional Ice Hockey Players and Relates to the Severity of Postconcussion Symptoms. Journal of neurotrauma. 2015;32(17):1294-300.doi:10.1089/neu.2014.3698
93. Kampfl A, Posmantur R, Nixon R, Grynspan F, Zhao X, Liu SJ, et al. mu-calpain activation and calpain-mediated cytoskeletal proteolysis following traumatic brain injury. Journal of neurochemistry. 1996;67(4):1575-83
94. Schoch KM, von Reyn CR, Bian J, Telling GC, Meaney DF, Saatman KE. Brain Injury-Induced Proteolysis Is Reduced in a Novel Calpastatin Overexpressing Transgenic Mouse. J Neurochem. 2013;125(6):909
95. Aleksandrova MA, Sukhinich KK. Astrocytes of the Brain: Retinue Plays the King. Russ J Dev Biol+. 2022;53(4):252-71.doi:10.1134/S1062360422040026
96. Sedmak G, Jovanov-Milošević N, Puskarjov M, Ulamec M, Krušlin B, Kaila K, et al. Developmental Expression Patterns of KCC2 and Functionally Associated Molecules in the Human Brain. Cerebral cortex. 2016;26(12):4574-89.doi:10.1093/cercor/bhv218
97. Colombo JA, Yanez A, Lipina SJ. Interlaminar astroglial processes in the cerebral cortex of non human primates: response to injury. J Hirnforsch. 1997;38(4):503-12
98. Verkhratsky A, Butt A, Li B, Illes P, Zorec R, Semyanov A, et al. Astrocytes in human central nervous system diseases: a frontier for new therapies. Signal Transduct Target Ther. 2023;8(1):396.doi:10.1038/s41392-023-01628-9
99. Caballero B, Bourdenx M, Luengo E, Diaz A, Sohn PD, Chen X, et al. Acetylated tau inhibits chaperone-mediated autophagy and promotes tau pathology propagation in mice. Nature Communications. 2021;12(1):2238.doi:10.1038/s41467-021-22501-9
100. Kabir F, Atkinson R, Cook AL, Phipps AJ, King AE. The role of altered protein acetylation in neurodegenerative disease. Frontiers in Aging Neuroscience. 2023;14.doi:10.3389/fnagi.2022.1025473

101. Lazarus RC, Buonora JE, Flora MN, Freedy JG, Holstein GR, Martinelli GP, et al. Protein Citrullination: A Proposed Mechanism for Pathology in Traumatic Brain Injury. Frontiers in neurology. 2015;6.doi:10.3389/fneur.2015.00204
102. Wang B, Fields L, Li L. Recent advances in characterization of citrullination and its implication in human disease research: From method development to network integration. Proteomics. 2023;23(21-22):e2200286.doi:10.1002/pmic.202200286
103. Ishigami A, Ohsawa T, Hiratsuka M, Taguchi H, Kobayashi S, Saito Y, et al. Abnormal accumulation of citrullinated proteins catalyzed by peptidylarginine deiminase in hippocampal extracts from patients with Alzheimer's disease. Journal of neuroscience research. 2005;80(1):120-8.doi:10.1002/jnr.20431
104. Wizeman JW, Nicholas AP, Ishigami A, Mohan R. Citrullination of glial intermediate filaments is an early response in retinal injury. Mol Vis. 2016;22:1137-55
105. Nicholas AP, Sambandam T, Echols JD, Barnum SR. Expression of citrullinated proteins in murine experimental autoimmune encephalomyelitis. The Journal of comparative neurology. 2005;486(3):254-66.doi:10.1002/cne.20527
106. Lee YB, Du S, Rhim H, Lee EB, Markelonis GJ, Oh TH. Rapid increase in immunoreactivity to GFAP in astrocytes in vitro induced by acidic pH is mediated by calcium influx and calpain I. Brain research. 2000;864(2):220-9
107. Popov A, Brazhe A, Denisov P, Sutyagina O, Li L, Lazareva N, et al. Astrocyte dystrophy in ageing brain parallels impaired synaptic plasticity. Aging Cell. 2021;20(3):e13334.doi:10.1111/acel.13334
108. Vagberg M, Norgren N, Dring A, Lindqvist T, Birgander R, Zetterberg H, et al. Levels and Age Dependency of Neurofilament Light and Glial Fibrillary Acidic Protein in Healthy Individuals and Their Relation to the Brain Parenchymal Fraction. PloS one. 2015;10(8):e0135886.doi:10.1371/journal.pone.0135886
109. Cooper JG, Stukas S, Ghodsi M, Ahmed N, Diaz-Arrastia R, Holmes DT, et al. Age specific reference intervals for plasma biomarkers of neurodegeneration and neurotrauma in a Canadian population. Clinical biochemistry. 2023;121-122:110680.doi:10.1016/j.clinbiochem.2023.110680
110. Li LM, Kodosaki E, Heslegrave A, Zetterberg H, Graham N, Zimmerman K, et al. High-dimensional proteomic analysis for pathophysiological classification of traumatic brain injury. Brain : a journal of neurology. 2024;148(3):1015-30.doi:10.1093/brain/awae305
111. Inekci D, Jonesco DS, Kennard S, Karsdal MA, Henriksen K. The potential of pathological protein fragmentation in blood-based biomarker development for dementia - with emphasis on Alzheimer's disease. Frontiers in neurology. 2015;6:90.doi:10.3389/fneur.2015.00090
112. Nielsen P, Olsen MH, Willer-Hansen RS, Hauerberg J, Johansen HK, Andersen AB, et al. Ventriculostomy-associated infection (VAI) in patients with acute brain injury-a retrospective study. Acta neurochirurgica. 2024;166(1):128.doi:10.1007/s00701-024-06018-w
113. Jha RM, Kochanek PM, Simard JM. Pathophysiology and treatment of cerebral edema in traumatic brain injury. Neuropharmacology. 2019;145(Pt B):230-46.doi:10.1016/j.neuropharm.2018.08.004
114. Shreiber DI, Bain AC, Ross DT, Smith DH, Gennarelli TA, McIntosh TK, et al. Experimental investigation of cerebral contusion: histopathological and immunohistochemical evaluation of dynamic cortical deformation. Journal of neuropathology and experimental neurology. 1999;58(2):153-64
115. Farkas O, Lifshitz J, Povlishock JT. Mechanoporation induced by diffuse traumatic brain injury: an irreversible or reversible response to injury? The Journal of neuroscience : the official journal of the Society for Neuroscience. 2006;26(12):3130-40
116. Barbee KA. Mechanical cell injury. Ann N Y Acad Sci. 2005;1066:67-84.doi:10.1196/annals.1363.006
117. Levine J, Kwon E, Sondej M, Paez P, Czerwieniec G, Ao Y, et al. Traumatically injured astrocytes release a proteomic signature modulated by STAT3 dependent cell survival. Glia. 2016;64:668-94.doi:10.1002/glia.22953

118. Dobson J, Kumar A, Willis LF, Tuma R, Higazi DR, Turner R, et al. Inducing protein aggregation by extensional flow. Proceedings of the National Academy of Sciences. 2017;114(18):4673-8.doi:doi:10.1073/pnas.1702724114
119. Rolleke U, Kumari P, Meyer R, Koster S. The unique biomechanics of intermediate filaments - From single filaments to cells and tissues. Current opinion in cell biology. 2023;85:102263.doi:10.1016/j.ceb.2023.102263
120. Karl J, Gottfried C, Tramontina F, Dunkley P, Rodnight R, Goncalves CA. GFAP phosphorylation studied in digitonin-permeabilized astrocytes: standardization of conditions. Brain research. 2000;853(1):32-40
121. Block J, Witt H, Candelli A, Peterman EJ, Wuite GJ, Janshoff A, et al. Nonlinear Loading-Rate-Dependent Force Response of Individual Vimentin Intermediate Filaments to Applied Strain. Phys Rev Lett. 2017;118(4):048101.doi:10.1103/PhysRevLett.118.048101
122. Guo J, Yang WT, Mai FY, Liang JR, Luo J, Zhou MC, et al. Unravelling oncosis: morphological and molecular insights into a unique cell death pathway. Front Immunol. 2024;15:1450998.doi:10.3389/fimmu.2024.1450998
123. Cao X, Zhang Y, Zou L, Xiao H, Chu Y, Chu X. Persistent oxygen-glucose deprivation induces astrocytic death through two different pathways and calpain-mediated proteolysis of cytoskeletal proteins during astrocytic oncosis. Neuroscience letters. 2010;479(2):118-22.doi:10.1016/j.neulet.2010.05.040
124. Ammendolia DA, Bement WM, Brumell JH. Plasma membrane integrity: implications for health and disease. BMC Biol. 2021;19(1):71.doi:10.1186/s12915-021-00972-y
125. Majno G, Joris I. Apoptosis, oncosis, and necrosis. An overview of cell death. The American journal of pathology. 1995;146(1):3-15
126. Chu X, Fu X, Zou L, Qi C, Li Z, Rao Y, et al. Oncosis, the possible cell death pathway in astrocytes after focal cerebral ischemia. Brain research. 2007;1149:157-64.doi:10.1016/j.brainres.2007.02.061
127. Loh KY, Wang Z, Liao P. Oncotic Cell Death in Stroke. Rev Physiol Biochem Pharmacol. 2019;176:37-64.doi:10.1007/112_2018_13
128. Bondarenko A, Chesler M. Calcium dependence of rapid astrocyte death induced by transient hypoxia, acidosis, and extracellular ion shifts. Glia. 2001;34(2):143-9
129. Vlodavsky E, Palzur E, Shehadeh M, Soustiel JF. Post-traumatic cytotoxic edema is directly related to mitochondrial function. Journal of cerebral blood flow and metabolism : official journal of the International Society of Cerebral Blood Flow and Metabolism. 2017;37(1):166-77.doi:10.1177/0271678X15621068
130. Bullock R, Maxwell WL, Graham DI, Teasdale GM, Adams JH. Glial swelling following human cerebral contusion: an ultrastructural study. Journal of neurology, neurosurgery, and psychiatry. 1991;54(5):427-34
131. Vespa P, Bergsneider M, Hattori N, Wu HM, Huang SC, Martin NA, et al. Metabolic crisis without brain ischemia is common after traumatic brain injury: a combined microdialysis and positron emission tomography study. Journal of cerebral blood flow and metabolism : official journal of the International Society of Cerebral Blood Flow and Metabolism. 2005;25(6):763-74.doi:10.1038/sj.jcbfm.9600073
132. Zhu X, Tao L, Tejima-Mandeville E, Qiu J, Park J, Garber K, et al. Plasmalemma permeability and necrotic cell death phenotypes after intracerebral hemorrhage in mice. Stroke; a journal of cerebral circulation. 2012;43(2):524-31.doi:10.1161/STROKEAHA.111.635672
133. Whalen MJ, Dalkara T, You Z, Qiu J, Bermpohl D, Mehta N, et al. Acute plasmalemma permeability and protracted clearance of injured cells after controlled cortical impact in mice. Journal of cerebral blood flow and metabolism : official journal of the International Society of Cerebral Blood Flow and Metabolism. 2008;28(3):490-505.doi:10.1038/sj.jcbfm.9600544

134. Li DR, Zhang F, Wang Y, Tan XH, Qiao DF, Wang HJ, et al. Quantitative analysis of GFAP- and S100 protein-immunopositive astrocytes to investigate the severity of traumatic brain injury. Leg Med (Tokyo). 2012;14(2):84-92.doi:10.1016/j.legalmed.2011.12.007
135. DeArmond SJ, Fajardo M, Naughton SA, Eng LF. Degradation of glial fibrillary acidic protein by a calcium dependent proteinase: an electroblot study. Brain research. 1983;262(2):275-82
136. Ciesielski-Treska J, Goetschy JF, Aunis D. Proteolytic degradation of vimentin and glial fibrillary acidic protein in rat astrocytes in primary culture. European journal of biochemistry / FEBS. 1984;138(3):465-71
137. Phillips CL, Fu D, Herring LE, Armao D, Snider NT. Calpain-mediated proteolysis of vimentin filaments is augmented in giant axonal neuropathy fibroblasts exposed to hypotonic stress. Front Cell Dev Biol. 2022;10:1008542.doi:10.3389/fcell.2022.1008542
138. Byun Y, Chen F, Chang R, Trivedi M, Green KJ, Cryns VL. Caspase cleavage of vimentin disrupts intermediate filaments and promotes apoptosis. Cell death and differentiation. 2001;8(5):443-50.doi:10.1038/sj.cdd.4400840
139. Metwally E, Al-Abbadi HA, Hussain T, Murtaza G, Abdellatif AM, Ahmed MF. Calpain signaling: from biology to therapeutic opportunities in neurodegenerative disorders. Front Vet Sci. 2023;10:1235163.doi:10.3389/fvets.2023.1235163
140. Liu G-Y, Xie W-L, Wang Y-T, Chen L, Xu Z-Z, Lv Y, et al. Calpain: the regulatory point of myocardial ischemia-reperfusion injury. Frontiers in Cardiovascular Medicine. 2023;Volume 10 - 2023.doi:10.3389/fcvm.2023.1194402
141. Dias C, Nylandsted J. Plasma membrane integrity in health and disease: significance and therapeutic potential. Cell Discovery. 2021;7(1):4.doi:10.1038/s41421-020-00233-2
142. Kilinc D, Gallo G, Barbee KA. Mechanical membrane injury induces axonal beading through localized activation of calpain. Experimental neurology. 2009;219(2):553-61.doi:10.1016/j.expneurol.2009.07.014
143. Weber JT. Altered calcium signaling following traumatic brain injury. Frontiers in pharmacology. 2012;3:60.doi:10.3389/fphar.2012.00060
144. Gafni J, Cong X, Chen SF, Gibson BW, Ellerby LM. Calpain-1 cleaves and activates caspase-7. The Journal of biological chemistry. 2009;284(37):25441-9.doi:10.1074/jbc.M109.038174
145. GOLL DE, THOMPSON VF, LI H, WEI W, CONG J. The Calpain System. Physiological Reviews. 2003;83(3):731-801.doi:10.1152/physrev.00029.2002
146. Pohl C, Dikic I. Cellular quality control by the ubiquitin-proteasome system and autophagy. Science. 2019;366(6467):818-22.doi:doi:10.1126/science.aax3769
147. Shields DC, Tyor WR, Deibler GE, Hogan EL, Banik NL. Increased calpain expression in activated glial and inflammatory cells in experimental allergic encephalomyelitis. Proceedings of the National Academy of Sciences. 1998;95(10):5768-72.doi:doi:10.1073/pnas.95.10.5768
148. Acarin L, Villapol S, Faiz M, Rohn TT, Castellano B, Gonzalez B. Caspase-3 activation in astrocytes following postnatal excitotoxic damage correlates with cytoskeletal remodeling but not with cell death or proliferation. Glia. 2007;55(9):954-65
149. Battaglia RA, Beltran AS, Delic S, Dumitru R, Robinson JA, Kabiraj P, et al. Site-specific phosphorylation and caspase cleavage of GFAP are new markers of Alexander disease severity. Elife. 2019;8.doi:10.7554/eLife.47789
150. Sambandam T, Belousova M, Accaviti-Loper MA, Blanquicett C, Guercello V, Raijmakers R, et al. Increased peptidylarginine deiminase type II in hypoxic astrocytes. Biochemical and biophysical research communications. 2004;325(4):1324-9.doi:10.1016/j.bbrc.2004.10.173
151. Algeciras ME, Takahara H, Bhattacharya SK. Mechanical stretching elevates peptidyl arginine deiminase 2 expression in astrocytes. Curr Eye Res. 2008;33(11):994-1001.doi:10.1080/02713680802447113

152. Jones JR, Kong L, Hanna MGt, Hoffman B, Krencik R, Bradley R, et al. Mutations in GFAP Disrupt the Distribution and Function of Organelles in Human Astrocytes. Cell Rep. 2018;25(4):947-58.e4.doi:10.1016/j.celrep.2018.09.083
153. Sosunov A, Olabarria M, Goldman JE. Alexander disease: an astrocytopathy that produces a leukodystrophy. Brain pathology. 2018;28(3):388-98.doi:10.1111/bpa.12601
154. Korley F, Pauls Q, Yeatts SD, Jones CMC, Corbett-Valade E, Silbergleit R, et al. Progesterone Treatment Does Not Decrease Serum Levels of Biomarkers of Glial and Neuronal Cell Injury in Moderate and Severe Traumatic Brain Injury Subjects: A Secondary Analysis of the Progesterone for Traumatic Brain Injury, Experimental Clinical Treatment (ProTECT) III Trial. J Neurotrauma. 2021;38(14):1953
155. Xiong L, Sun L, Liu S, Zhu X, Teng Z, Yan J. The Protective Roles of Urinary Trypsin Inhibitor in Brain Injury Following Fat Embolism Syndrome in a Rat Model. Cell Transplant. 2019;28(6):704-12.doi:10.1177/0963689718814766
156. Fereidoni M, Sabouni F, Moghimi A, Hosseini S. The effects of trypsin on rat brain astrocyte activation. Iran J Neurol. 2013;12(4):129-35
157. Gae DD, Budamagunta MS, Hess JF, McCarrick RM, Lorigan GA, FitzGerald PG, et al. Completion of the Vimentin Rod Domain Structure Using Experimental Restraints: A New Tool for Exploring Intermediate Filament Assembly and Mutations. Structure. 2019;27(10):1547-60.e4.doi:10.1016/j.str.2019.07.011
158. Strelkov SV, Herrmann H, Geisler N, Wedig T, Zimbelmann R, Aebi U, et al. Conserved segments 1A and 2B of the intermediate filament dimer: their atomic structures and role in filament assembly. The EMBO journal. 2002;21(6):1255-66.doi:https://doi.org/10.1093/emboj/21.6.1255
159. Iliff JJ, Lee H, Yu M, Feng T, Logan J, Nedergaard M, et al. Brain-wide pathway for waste clearance captured by contrast-enhanced MRI. The Journal of clinical investigation. 2013;123(3):1299-309.doi:10.1172/JCI67677
160. Benedet AL, Milà-Alomà M, Vrillon A, Ashton NJ, Pascoal TA, Lussier F, et al. Differences Between Plasma and Cerebrospinal Fluid Glial Fibrillary Acidic Protein Levels Across the Alzheimer Disease Continuum. JAMA neurology. 2021;78(12):1471-83.doi:10.1001/jamaneurol.2021.3671
161. Hagemann TL, Boelens WC, Wawrousek EF, Messing A. Suppression of GFAP toxicity by alphaB-crystallin in mouse models of Alexander disease. Human molecular genetics. 2009;18(7):1190-9.doi:10.1093/hmg/ddp013
162. Rai M, Curley M, Coleman Z, Nityanandam A, Jiao J, Graca FA, et al. Analysis of proteostasis during aging with western blot of detergent-soluble and insoluble protein fractions. STAR Protoc. 2021;2(3):100628.doi:10.1016/j.xpro.2021.100628
163. Escartin C, Galea E, Lakatos A, O'Callaghan JP, Petzold GC, Serrano-Pozo A, et al. Reactive astrocyte nomenclature, definitions, and future directions. Nat Neurosci. 2021;24(3):312-25.doi:10.1038/s41593-020-00783-4
164. Madias MI, Stessman LN, Warlof SJ, Kudryashev JA, Kwon EJ. Spatial Measurement and Inhibition of Calpain Activity in Traumatic Brain Injury with an Activity-Based Nanotheranostic Platform. ACS Nano. 2024;18(37):25565-76.doi:10.1021/acsnano.4c06052
165. Adamczak SE, de Rivero Vaccari JP, Dale G, Brand FJ, 3rd, Nonner D, Bullock MR, et al. Pyroptotic neuronal cell death mediated by the AIM2 inflammasome. Journal of cerebral blood flow and metabolism : official journal of the International Society of Cerebral Blood Flow and Metabolism. 2014;34(4):621-9.doi:10.1038/jcbfm.2013.236
166. Harter L, Keel M, Hentze H, Leist M, Ertel W. Caspase-3 activity is present in cerebrospinal fluid from patients with traumatic brain injury. Journal of neuroimmunology. 2001;121(1-2):76-8
167. Diaz-Arrastia R, Kochanek PM, Bergold P, Kenney K, Marx CE, Grimes CJ, et al. Pharmacotherapy of traumatic brain injury: state of the science and the road forward: report of the Department of Defense

Neurotrauma Pharmacology Workgroup. Journal of neurotrauma. 2014;31(2):135-58.doi:10.1089/neu.2013.3019
168. Levine J, Kwon E, Paez P, Yan W, Czerwieniec G, Loo JA, et al. Traumatically injured astrocytes release a proteomic signature modulated by STAT3-dependent cell survival. Glia. 2015.doi:10.1002/glia.22953
169. Seidenfaden S-C, Kjerulff JL, Juul N, Kirkegaard H, Fogh Møller M, Bloch Münster A-M, et al. Temporal Changes in Serum S100B Levels From Prehospital to Early In-Hospital Sampling in Patients Suffering Traumatic Brain Injury. Frontiers in neurology. 2022;Volume 13 - 2022.doi:10.3389/fneur.2022.800015
170. Lisi I, Moro F, Mazzone E, Marklund N, Pischiutta F, Kobeissy F, et al. Exploiting blood-based biomarkers to align preclinical models with human traumatic brain injury. Brain : a journal of neurology. 2024.doi:10.1093/brain/awae350
171. Zhou Z, Zhao T, Gardus J, Wen Q, Feng Y, DeLorenzo C, et al. Quantifying Ventricular CSF Clearance in the Human Brain Using Dynamic 18F-FDG PET: Insights into Age-Related Glymphatic Impairment. medRxiv. 2025:2025.04.07.25325241.doi:10.1101/2025.04.07.25325241
172. Gardner RC, Dams-O'Connor K, Morrissey MR, Manley GT. Geriatric Traumatic Brain Injury: Epidemiology, Outcomes, Knowledge Gaps, and Future Directions. Journal of neurotrauma. 2017;35(7):889-906.doi:10.1089/neu.2017.5371
173. Chen CP, Chen RL, Preston JE. The influence of cerebrospinal fluid turnover on age-related changes in cerebrospinal fluid protein concentrations. Neuroscience letters. 2010;476(3):138-41.doi:10.1016/j.neulet.2010.04.015
174. Kim JH, Im JG, Park SH. Measurement of changes in cerebrospinal fluid pulsation after traumatic brain injury using echo-planar imaging-based functional MRI. NMR in biomedicine. 2024;37(3):e5061.doi:10.1002/nbm.5061
175. Bolte AC, Dutta AB, Hurt ME, Smirnov I, Kovacs MA, McKee CA, et al. Meningeal lymphatic dysfunction exacerbates traumatic brain injury pathogenesis. Nature Communications. 2020;11(1):4524.doi:10.1038/s41467-020-18113-4
176. Xiong G, Elkind JA, Kundu S, Smith CJ, Antunes MB, Tamashiro E, et al. Traumatic brain injury-induced ependymal ciliary loss decreases cerebral spinal fluid flow. Journal of neurotrauma. 2014;31(16):1396-404.doi:10.1089/neu.2013.3110
177. Yeh P-H, Lippa SM, Brickell TA, Ollinger J, French LM, Lange RT. Longitudinal changes of white matter microstructure following traumatic brain injury in U.S. military service members. Brain Communications. 2022;4(3).doi:10.1093/braincomms/fcac132
178. Batista L, Stence NV, Mirsky DM, Lewis T, Graber S, Ghebrechristos HE, et al. Cytotoxic edema is associated with injury severity but not abusive mechanism in young children with traumatic brain injury. Child Abuse & Neglect. 2025;161:107312.doi:https://doi.org/10.1016/j.chiabu.2025.107312
179. Newcombe VF, Williams GB, Outtrim JG, Chatfield D, Abate MG, Geeraerts T, et al. Microstructural Basis of Contusion Expansion in Traumatic Brain Injury: Insights from Diffusion Tensor Imaging. Journal of Cerebral Blood Flow & Metabolism. 2013;33(6):855-62.doi:10.1038/jcbfm.2013.11
180. Turtzo LC, Luby M, Jikaria N, Griffin AD, Greenman D, Bokkers RPH, et al. Cytotoxic Edema Associated with Hemorrhage Predicts Poor Outcome after Traumatic Brain Injury. Journal of neurotrauma. 2021;38(22):3107-18.doi:10.1089/neu.2021.0037
181. Korley FK, Jain S, Sun X, Puccio AM, Yue JK, Gardner RC, et al. Prognostic value of day-of-injury plasma GFAP and UCH-L1 concentrations for predicting functional recovery after traumatic brain injury in patients from the US TRACK-TBI cohort: an observational cohort study. The Lancet Neurology. 2022;21(9):803-13.doi:10.1016/S1474-4422(22)00256-3

182. Nylén K, Ost M, Csajbok LZ, Nilsson I, Blennow K, Nellgård B, et al. Increased serum-GFAP in patients with severe traumatic brain injury is related to outcome. Journal of the neurological sciences. 2006;240(1-2):85-91.doi:10.1016/j.jns.2005.09.007
183. Kulbe JR, Jain S, Nelson LD, Korley FK, Mukherjee P, Sun X, et al. Association of day-of-injury plasma glial fibrillary acidic protein concentration and six-month posttraumatic stress disorder in patients with mild traumatic brain injury. Neuropsychopharmacology. 2022;47(13):2300-8.doi:10.1038/s41386-022-01359-5
184. Wilson JE, Shinall MC, Jr., Leath TC, Wang L, Harrell FE, Jr., Wilson LD, et al. Worse Than Death: Survey of Public Perceptions of Disability Outcomes After Hypothetical Traumatic Brain Injury. Ann Surg. 2021;273(3):500-6.doi:10.1097/SLA.0000000000003389
185. Yamal JM, Aisiku IP, Hannay HJ, Brito FA, Robertson CS. Disability Rating Scale in the First Few Weeks After a Severe Traumatic Brain Injury as a Predictor of 6-Month Functional Outcome. Neurosurgery. 2021;88(3):619-26.doi:10.1093/neuros/nyaa474
186. Bhattacharyay S, Caruso PF, Åkerlund C, Wilson L, Stevens RD, Menon DK, et al. Mining the contribution of intensive care clinical course to outcome after traumatic brain injury. npj Digital Medicine. 2023;6(1):154.doi:10.1038/s41746-023-00895-8

Thumbnail

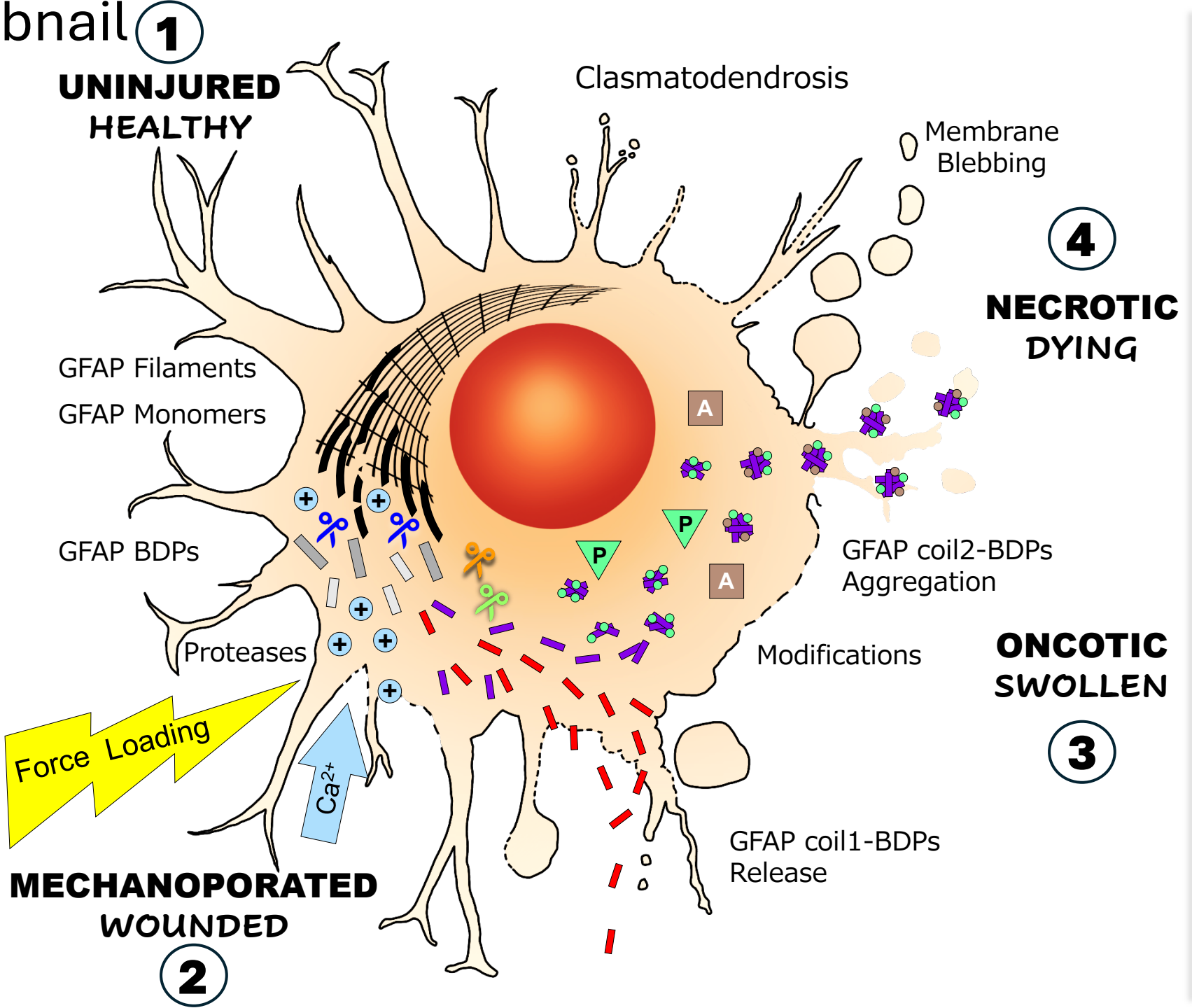

Symbol key

- GFAP Filaments
- GFAP Monomers +/- break
- Large GFAP-BDPs (42-49kDa)
- Calpain GFAP-BDPs (37-39kDa)
- Small GFAP Coil1-BDPs
- Small GFAP Coil2-BDPs
- GFAP Aggregates
- Calcium
- Peptidyl deiminases, PADs
- Citrullination
- Acetyltransferases
- Acetylation
- Calpain
- Caspase
- Endogenous Trypsin activity

Figure 1

A

GFAP TBI CSF

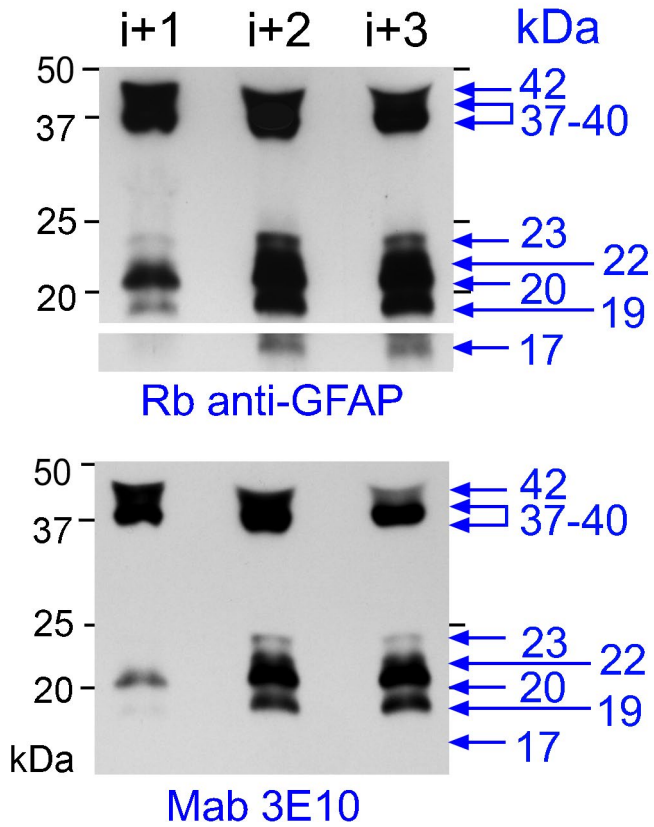

15% gel, 56ul CSF

B

GFAP Breakdown Products in TBI

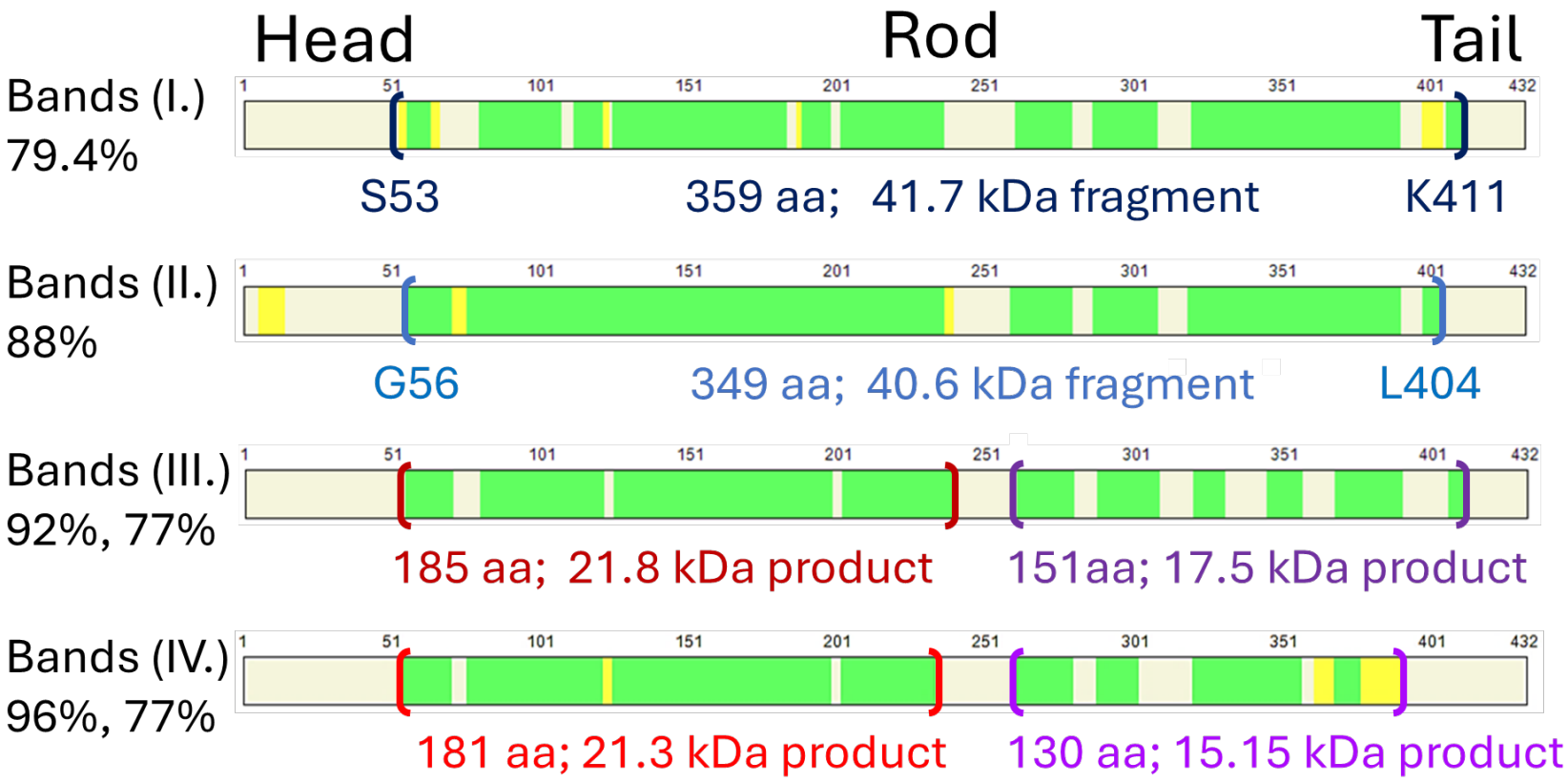

C

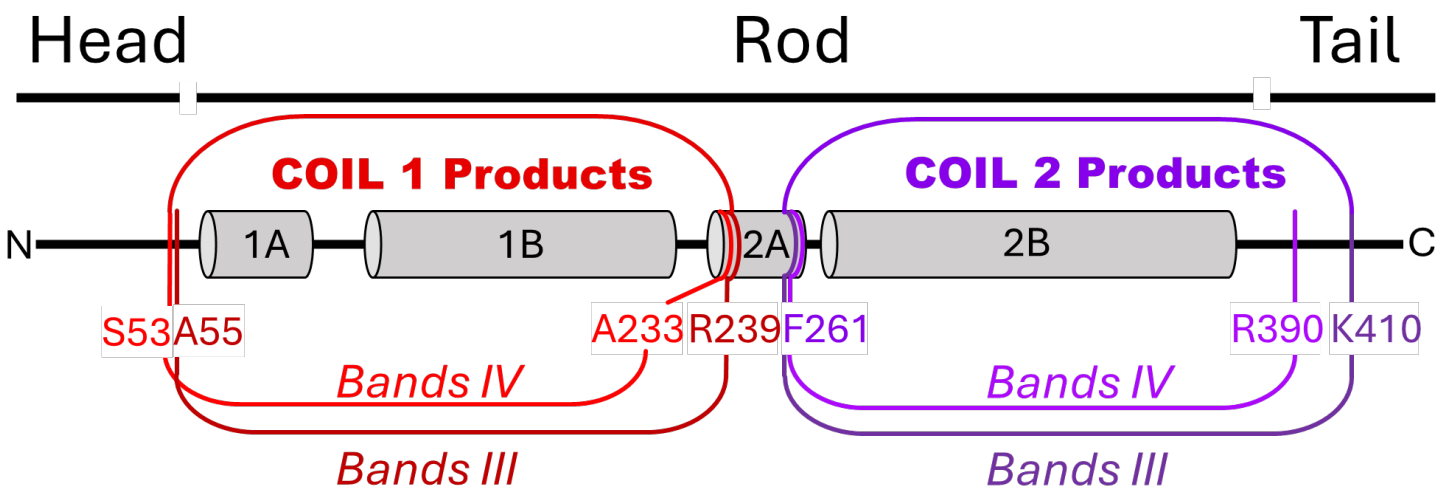

Figure 2

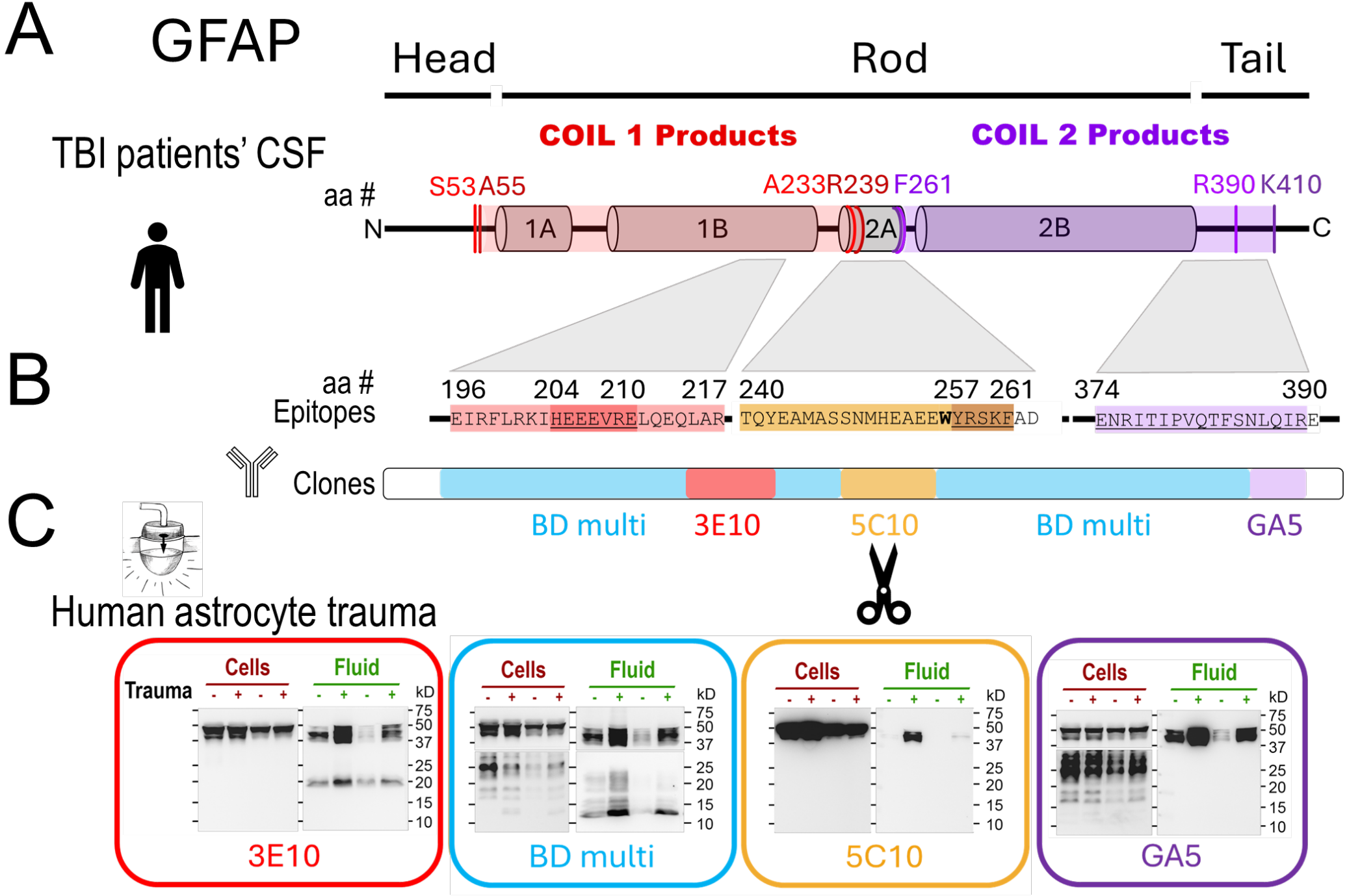
A
GFAP
Head
Rod
Tail
TBI patients' CSF
COIL 1 Products
COIL 2 Products
aa #
S53 A55
A233 R239 F261
R390 K410
N
1A
1B
2A
2B
C
B
aa #
196 204 210 217 240 257 261 374 390
Epitopes
EIRFLRKIHEEEVRELQEQLAR
TQYEAMASSNMHEAEEWYRSKFAD
ENRITIPVQTFSNLQIRE
Clones
BD multi
3E10
5C10
BD multi
GA5
C
Human astrocyte trauma
Trauma
Cells
Fluid
kD
75
50
37
25
20
15
10
3E10
BD multi
5C10
GA5

Figure 3

A

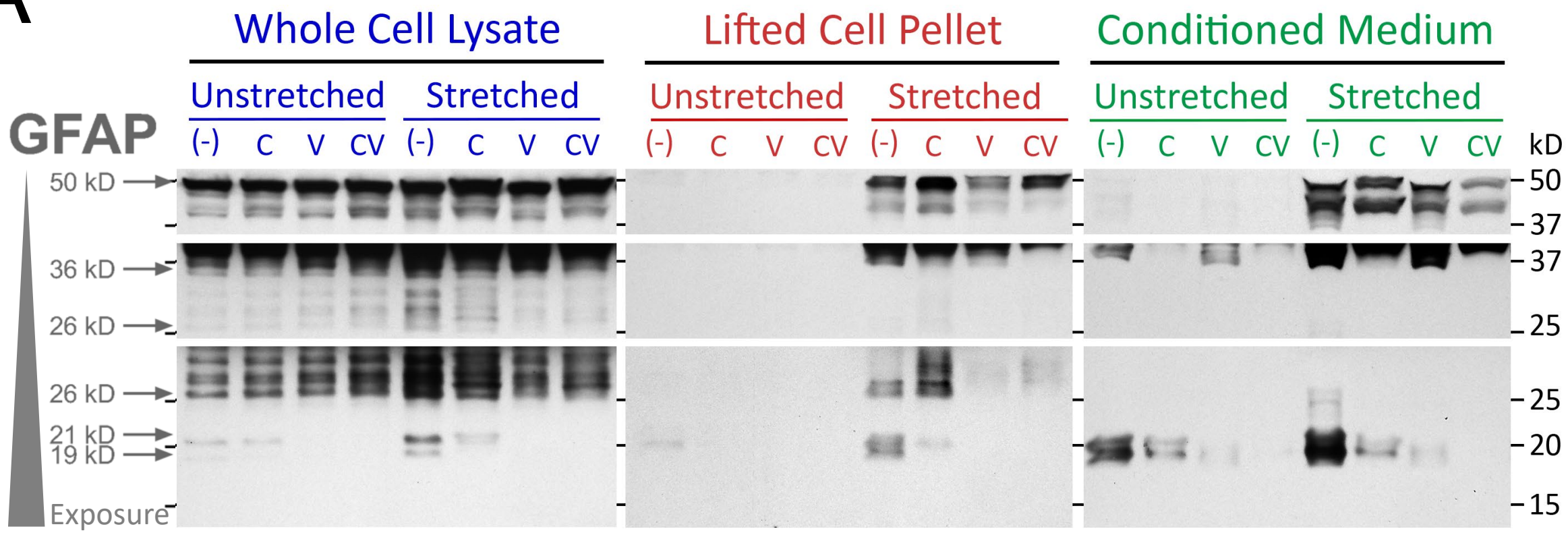
Whole Cell Lysate
Lifted Cell Pellet
Conditioned Medium
Unstretched
Stretched
Unstretched
Stretched
Unstretched
Stretched
GFAP
(-) c v cv (-) c v cv
(-) c v cv (-) c v cv
(-) c v cv (-) c v cv
kD
50 kD
36 kD
26 kD
26 kD
21 kD
19 kD
Exposure
50
37
37
25
25
20
15

Figure 3

B

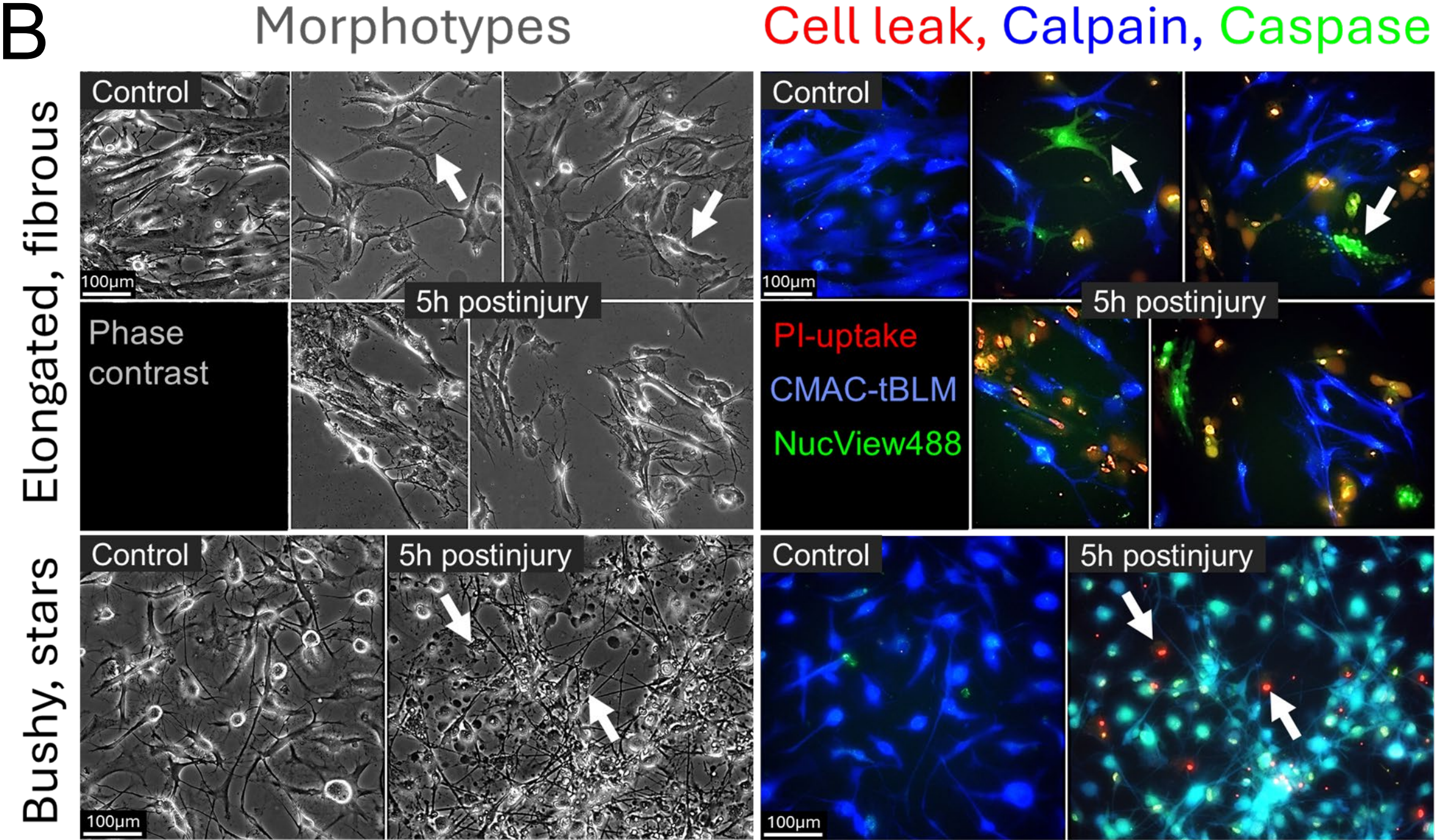
Morphotypes
Cell leak, Calpain, Caspase
Elongated, fibrous
Bushy, stars
Control
5h postinjury
Phase contrast
100µm
PI-uptake
CMAC-tBLM
NucView488

Figure 3

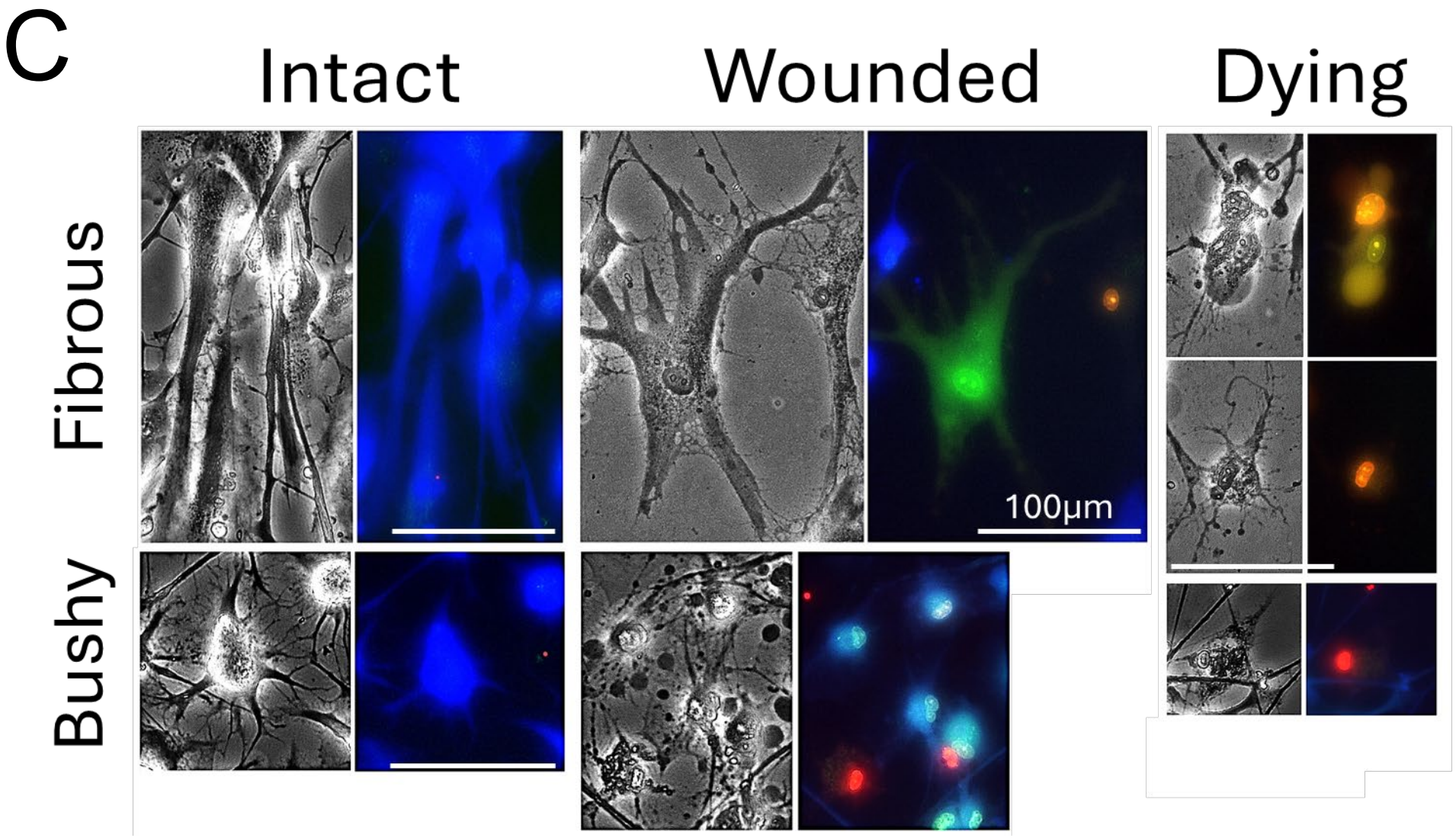

Figure 4

A

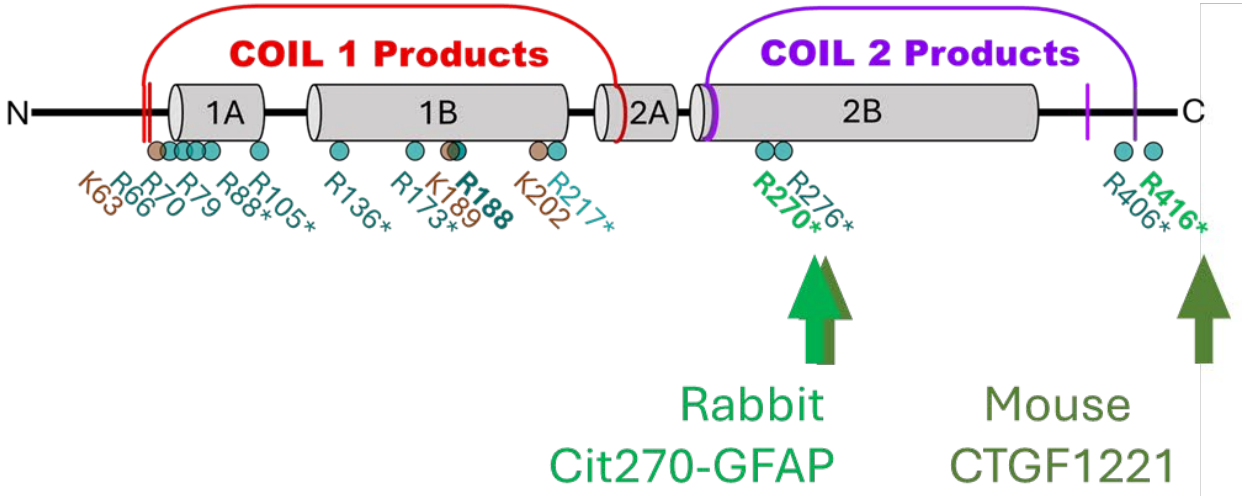

- 13 Citrullinated arginine residues
- 5 Acetylated lysine residues

B

Citrullinated GFAP Unmodified GFAP

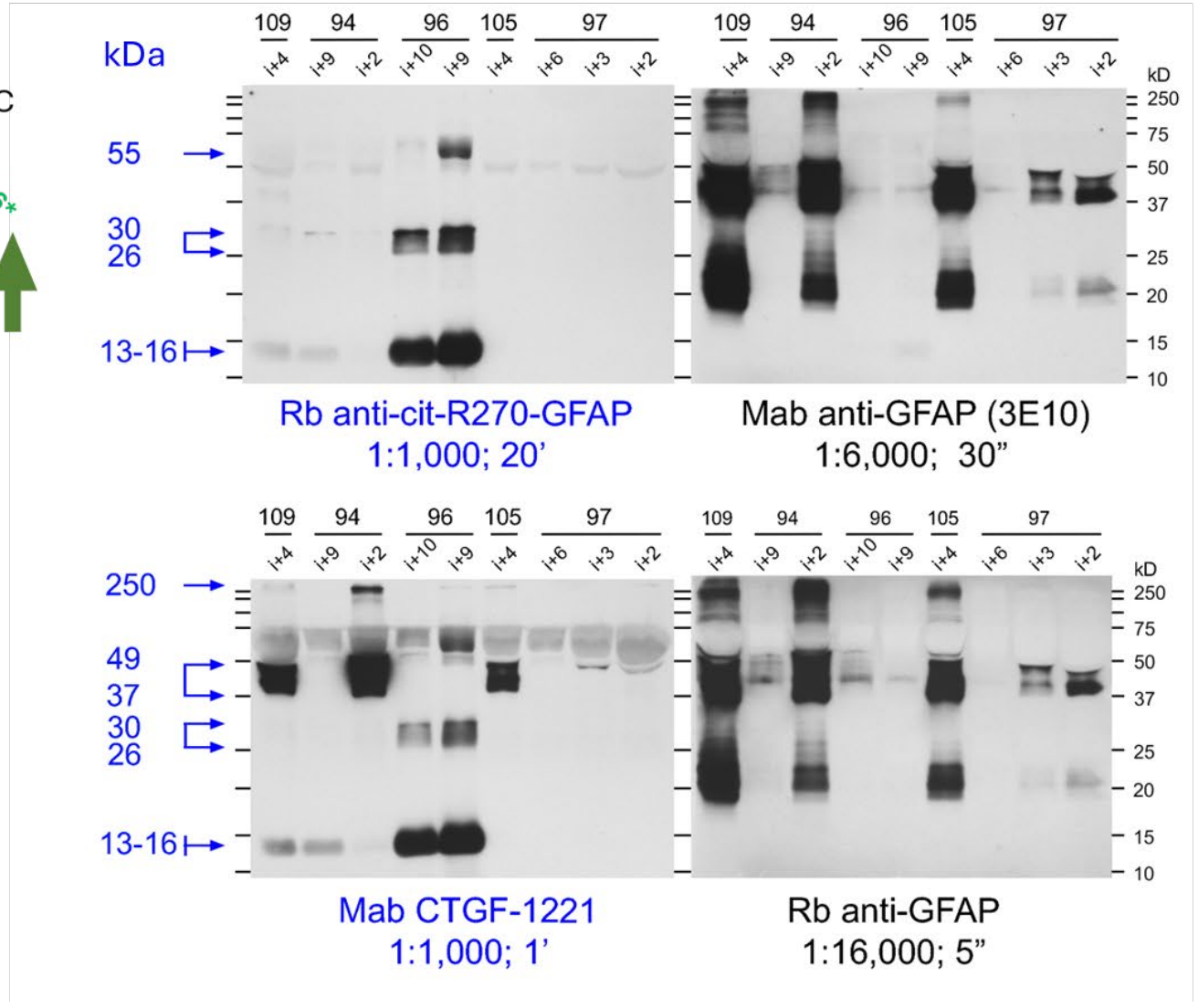

Figure 5

A

Control

Trauma

Unstretched

5h post-stretch

24h post-stretch

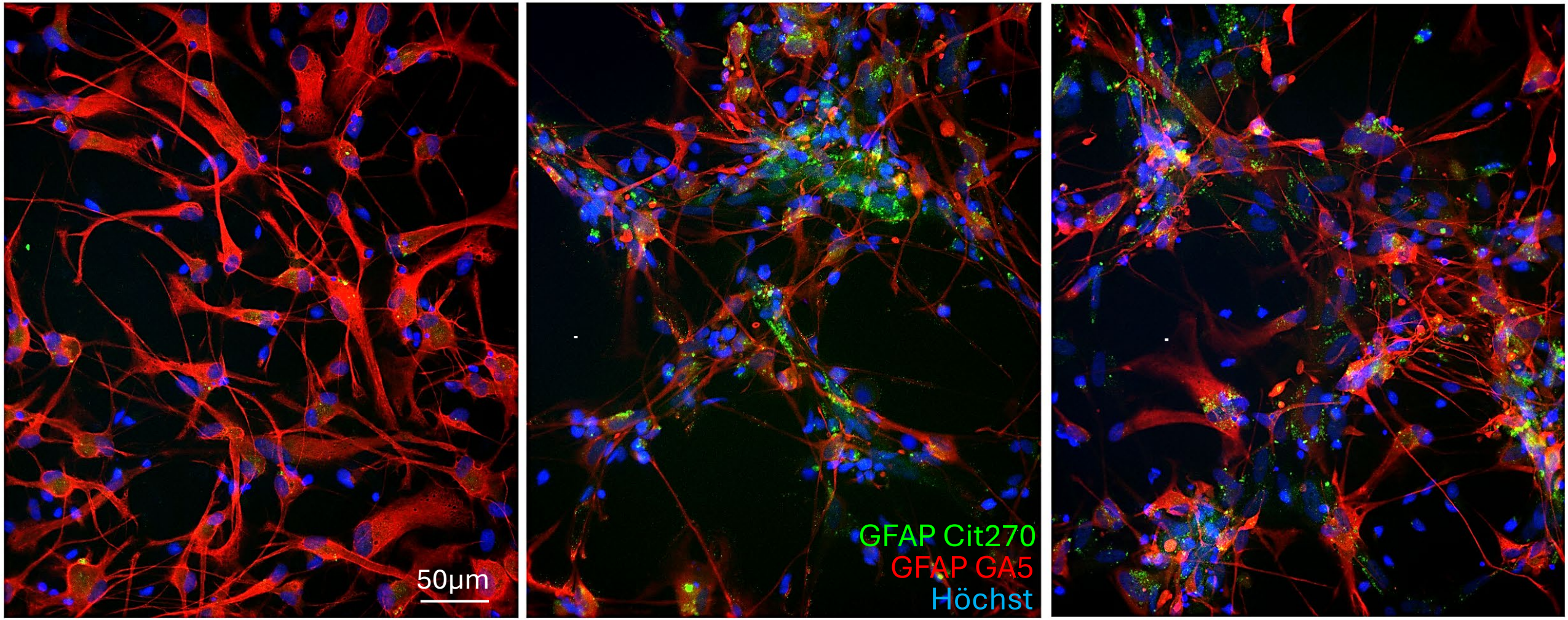

Figure 5

B

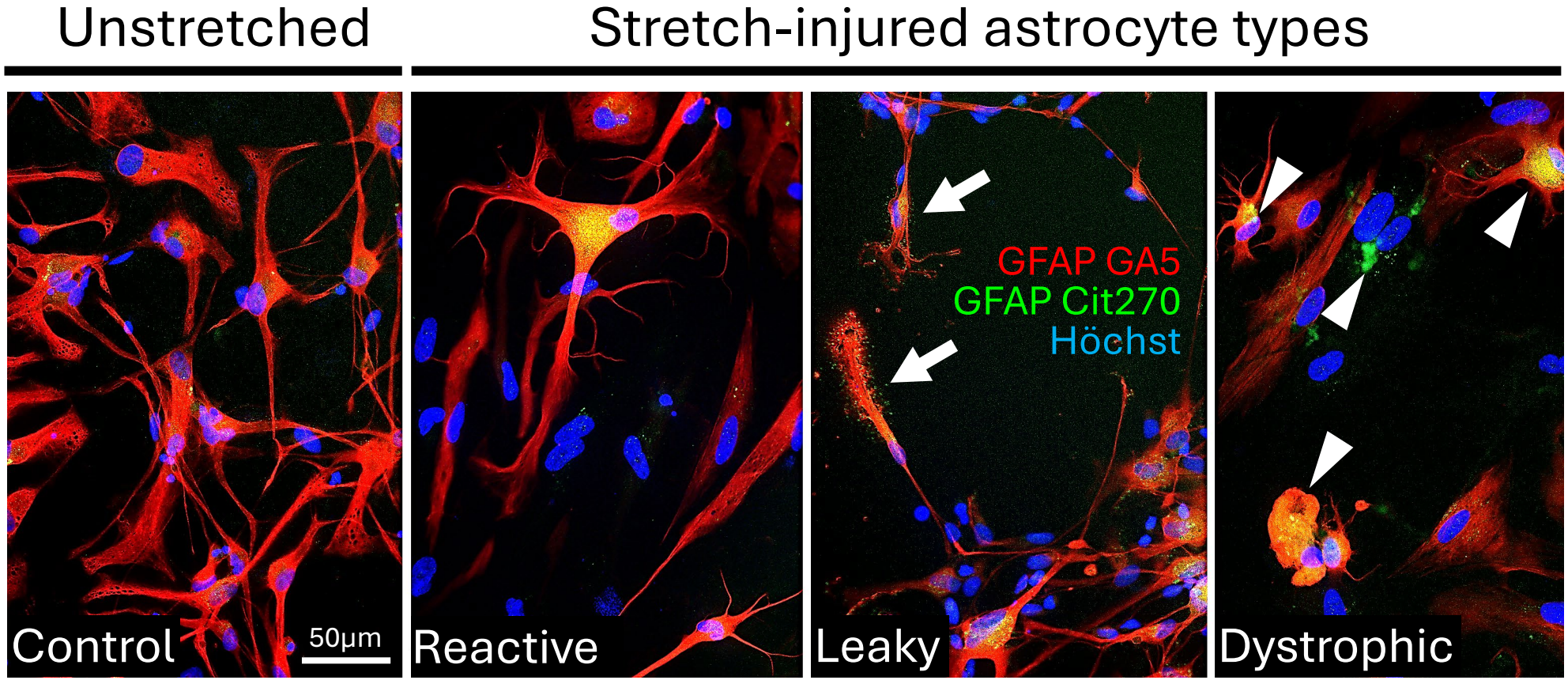
Unstretched
Stretch-injured astrocyte types
Control
50µm
Reactive
GFAP GA5
GFAP Cit270
Höchst
Leaky
Dystrophic

Figure 6

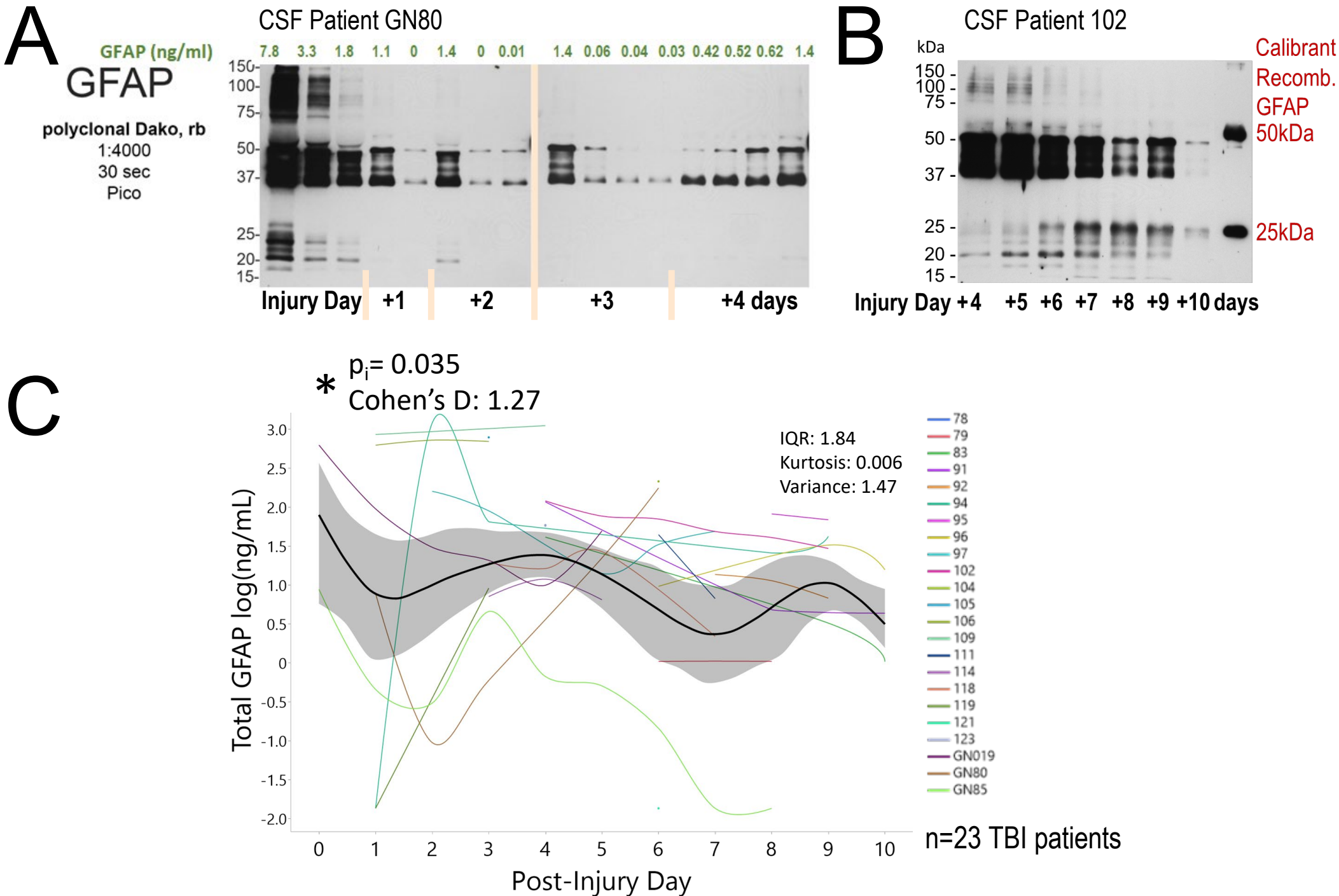
A
GFAP (ng/ml)
GFAP
polyclonal Dako, rb
1:4000
30 sec
Pico
CSF Patient GN80
7.8 3.3 1.8 1.1 0 1.4 0 0.01 1.4 0.06 0.04 0.03 0.42 0.52 0.62 1.4
150
100
75
50
37
25
20
15
Injury Day +1 +2 +3 +4 days
B
CSF Patient 102
kDa
150
100
75
50
37
25
20
15
Calibrant
Recomb.
GFAP
50kDa
25kDa
Injury Day +4 +5 +6 +7 +8 +9 +10 days
C
* p_i= 0.035
Cohen's D: 1.27
IQR: 1.84
Kurtosis: 0.006
Variance: 1.47
Total GFAP log(ng/mL)
3.0
2.5
2.0
1.5
1.0
0.5
0
-0.5
-1.0
-1.5
-2.0
0 1 2 3 4 5 6 7 8 9 10
Post-Injury Day
78
79
83
91
92
94
95
96
97
102
104
105
106
109
111
114
118
119
121
123
GN019
GN80
GN85
n=23 TBI patients

Figure 6 (D-H)

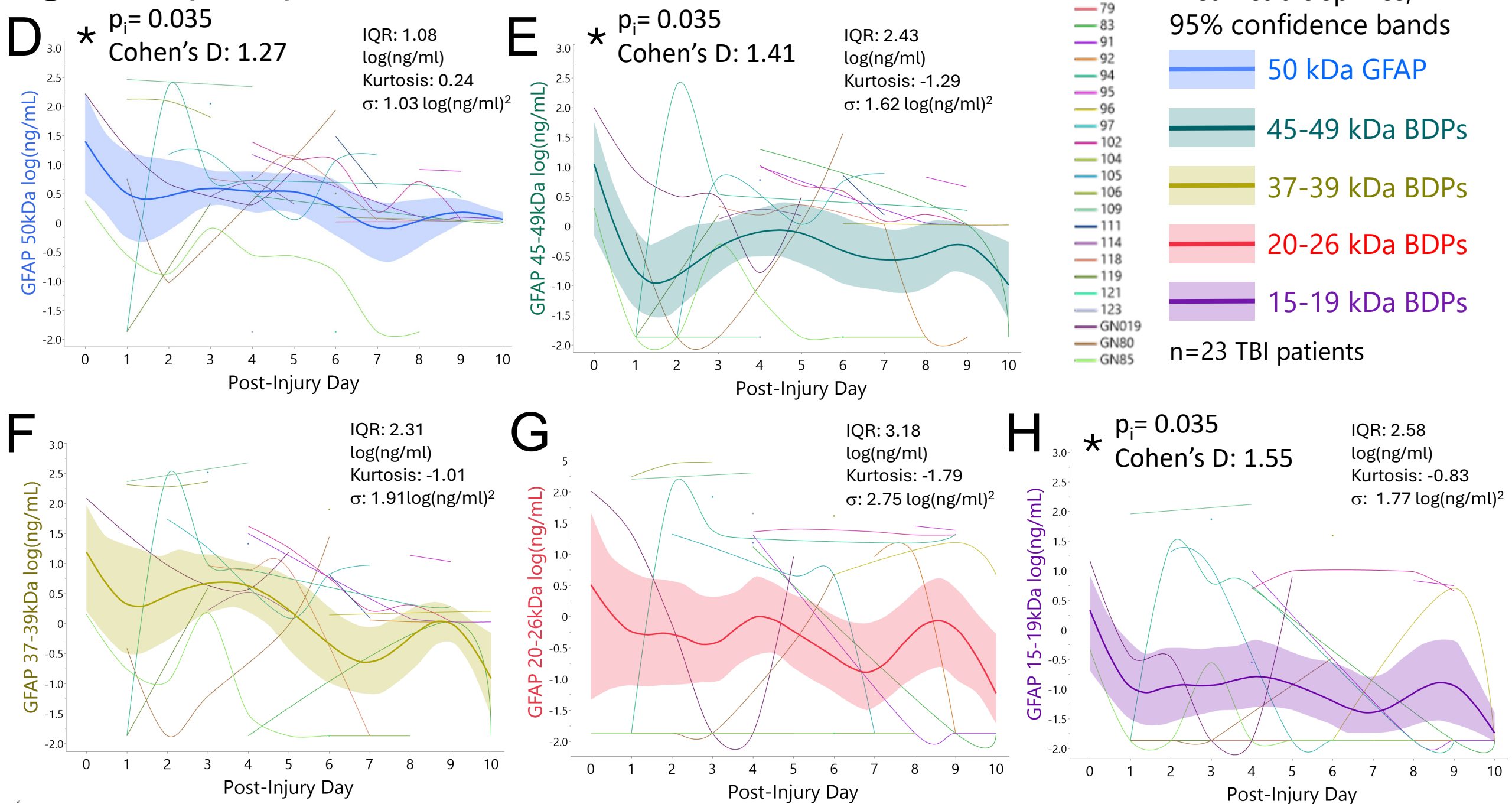
D
* p_i= 0.035
Cohen's D: 1.27
IQR: 1.08
log(ng/ml)
Kurtosis: 0.24
σ: 1.03 log(ng/ml)^2
GFAP 50kDa log(ng/mL)
Post-Injury Day
E
* p_i= 0.035
Cohen's D: 1.41
IQR: 2.43
log(ng/ml)
Kurtosis: -1.29
σ: 1.62 log(ng/ml)^2
GFAP 45-49kDa log(ng/mL)
Post-Injury Day
78
79
83
91
92
94
95
96
97
102
104
105
106
109
111
114
118
119
121
123
GN019
GN80
GN85
Mean cubic splines,
95% confidence bands
50 kDa GFAP
45-49 kDa BDPs
37-39 kDa BDPs
20-26 kDa BDPs
15-19 kDa BDPs
n=23 TBI patients
F
IQR: 2.31
log(ng/ml)
Kurtosis: -1.01
σ: 1.91log(ng/ml)^2
GFAP 37-39kDa log(ng/mL)
Post-Injury Day
G
IQR: 3.18
log(ng/ml)
Kurtosis: -1.79
σ: 2.75 log(ng/ml)^2
GFAP 20-26kDa log(ng/mL)
Post-Injury Day
H
* p_i= 0.035
Cohen's D: 1.55
IQR: 2.58
log(ng/ml)
Kurtosis: -0.83
σ: 1.77 log(ng/ml)^2
GFAP 15-19kDa log(ng/mL)
Post-Injury Day

Figure 7

A

Pearsons Correlation Coefficients

	45-49kDa	40-42kDa	37-39kDa	20-26kDa	15-19kDa
50kDa	0.575	0.637	0.822	0.604	0.529
45-49kDa		0.596	0.589	0.413	0.422
40-42kDa			0.726	0.549	0.363
37-39kDa				0.714	0.567
20-26kDa					0.685
15-19kDa					

B

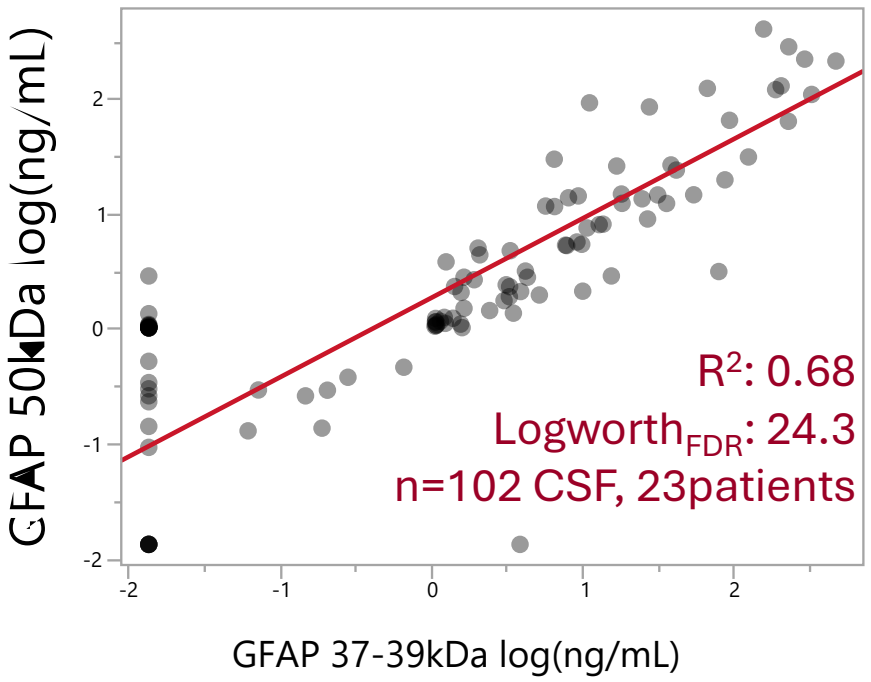

C

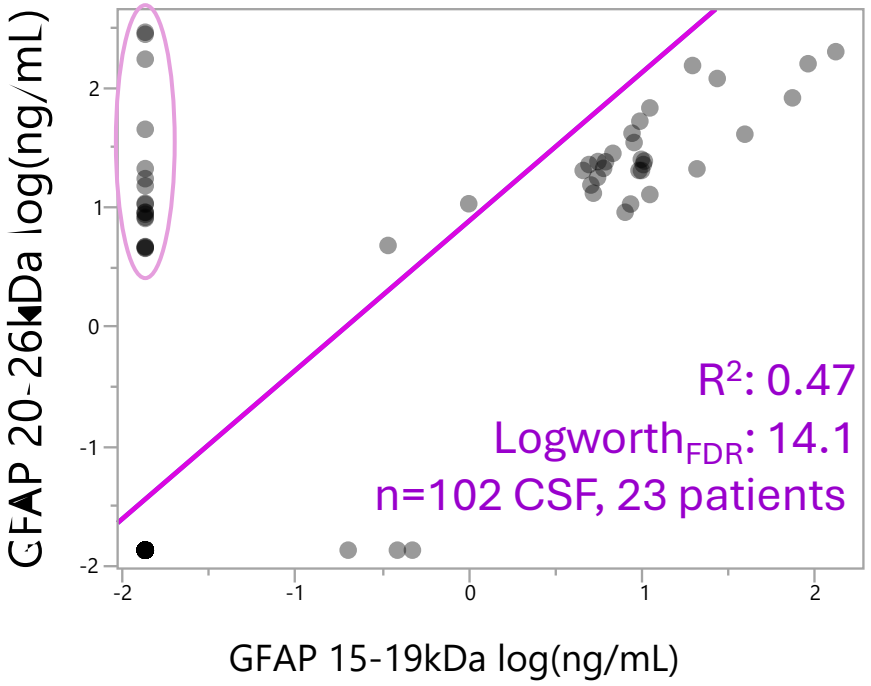

Figure 8

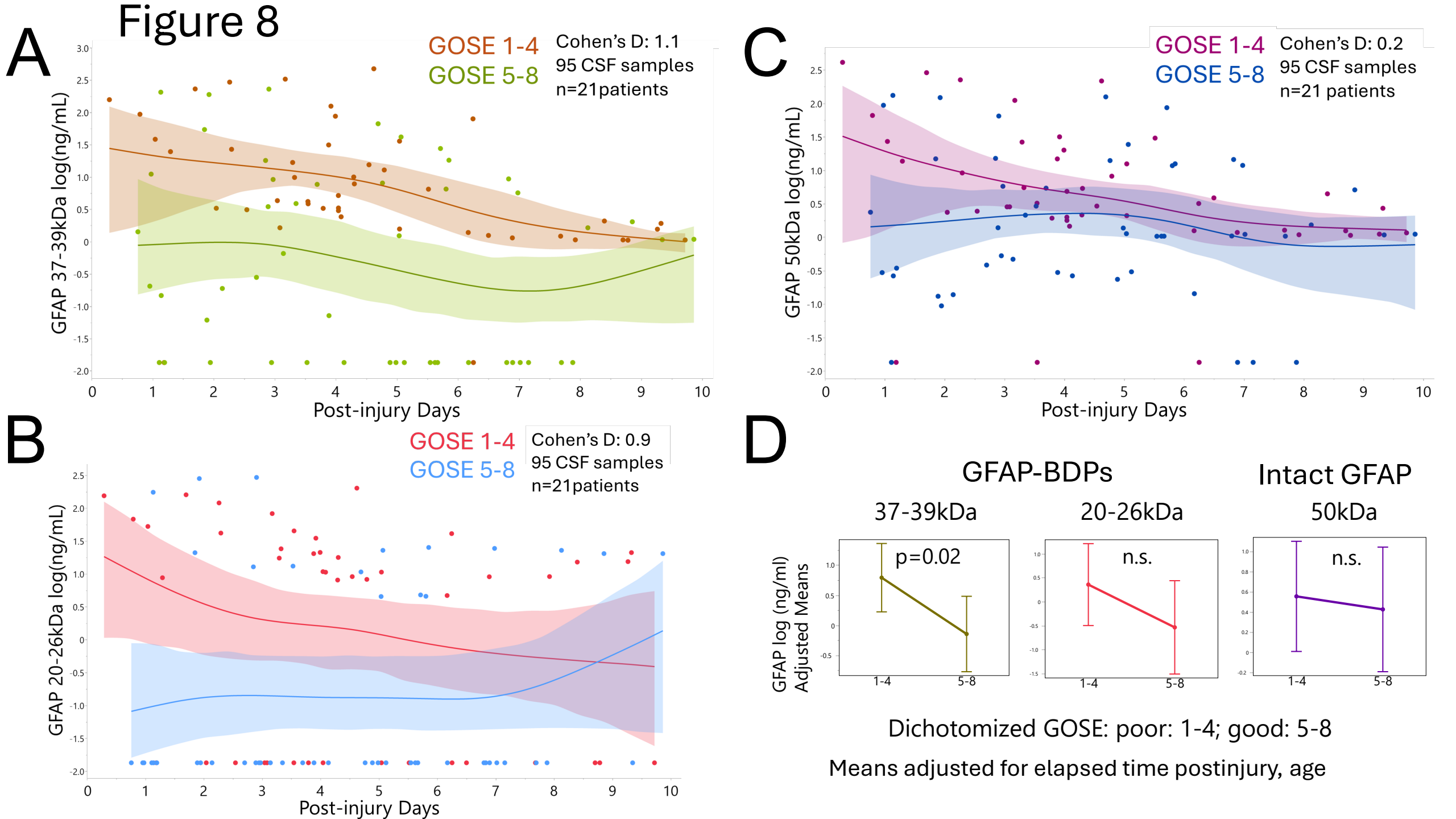
A
GOSE 1-4
GOSE 5-8
Cohen's D: 1.1
95 CSF samples
n=21patients
GFAP 37-39kDa log(ng/mL)
Post-injury Days
B
GOSE 1-4
GOSE 5-8
Cohen's D: 0.9
95 CSF samples
n=21patients
GFAP 20-26kDa log(ng/mL)
Post-injury Days
C
GOSE 1-4
GOSE 5-8
Cohen's D: 0.2
95 CSF samples
n=21 patients
GFAP 50kDa log(ng/mL)
Post-injury Days
D
GFAP-BDPs
Intact GFAP
37-39kDa
20-26kDa
50kDa
GFAP log (ng/ml)
Adjusted Means
p=0.02
n.s.
n.s.
1-4
5-8
Dichotomized GOSE: poor: 1-4; good: 5-8
Means adjusted for elapsed time postinjury, age